

## RADIATIVE DECAY OF EDGE STATES IN FLOQUET MEDIA

SAMEH N. HAMEEDI, AMIR SAGIV, AND MICHAEL I. WEINSTEIN

**ABSTRACT.** We consider the effect of time-periodic forcing on a one-dimensional Schrödinger equation with a topologically protected defect (edge) mode. The unforced system models a domain-wall or dislocation defect in a periodic structure, and it supports a defect mode which bifurcates from the Dirac point (linear band crossing) of the underlying bulk medium. We study the robustness of this state against time-periodic forcing of the type that arises in the study of Floquet Topological Insulators in condensed matter, photonics, and cold-atoms systems. Our numerical simulations demonstrate that under time-periodic forcing of sufficiently high frequency, the defect state undergoes radiative leakage of its energy away from the interface into the bulk; the time-decay is exponential on a time-scale proportional to the inverse square of the forcing amplitude. The envelope dynamics of our Floquet system are approximately governed, on long time scales, by an effective (homogenized) periodically-forced Dirac equation. Multiple scale analysis of the effective envelope dynamics yields an expansion of the radiating solution, which shows excellent agreement with our numerical simulations.

## 1. INTRODUCTION

Consider wave propagation in a periodic and non-dissipative medium. In such a medium, spatially localized defects or extended interfaces often give rise to *defect modes*, states in which energy can concentrate. These are described by time-harmonic solutions of the underlying wave equations. In the field of topological insulators, a class of defect modes of particular interest are those whose existence is tied to a linear or conical touching of spectral bands (*Dirac points*) of an underlying bulk periodic medium, and whose robustness against perturbations is owed to the breaking of time reversal symmetry and the associated non-triviality of a topological invariant associated with the band structure. Such robust states are of broad interest in applications to storage and transmission of information.

Recently there has been great interest in *Floquet materials*, in which time-periodic forcing is applied to spatially periodic media in settings like those above [6, 30]. As with other perturbations which break time-reversal symmetry, Floquet systems give rise to chirality (uni-directionality) of modes and topological stability against defects. However, Floquet materials have the advantage of a larger design-space, allowing one to tune a system to convert between being topologically trivial and non-trivial [8], and even be more conducive to nonlinearly localized modes [1, 2, 21, 29]. Floquet systems also display a greater variety of topological properties than their static counterparts; these systems are periodic in one additional dimension and hence have a larger family of topological invariants defined on their high dimensional Brillouin zone [34, 36].

The topological robustness of defect states in such systems has been explored in experiments [16, 30, 31, 41], and theoretically, mainly in the context of tight-binding

(discrete) models [4, 8, 17, 35]. Simulations of models of one- and two-dimensional optical systems show Floquet edge modes that persist over long propagation distances, but eventually disperse into the bulk [18, 20, 32].

*In this article we show, in a class of models, that defect states which exhibit topological robustness in the autonomous (unforced) setting are only metastable against time-periodic parametric forcing; on a sufficiently long time scale, such states resonantly couple to bulk (radiation) modes and radiate their energy away from the defect and into the bulk. We derive an asymptotic theory based on parametrically forced effective (homogenized) Dirac operator, which gives predictions in agreement with our numerical simulations of both the Schrödinger and the effective Dirac models.*

In contrast to the common assertions in the topological insulators literature [4, 8, 17, 35], our results suggest that no true “Floquet edge modes” exist in generic continuum models. Rather, only metastable modes which eventually decay into the bulk due to the resonant effect of forcing.

**1.1. Overview of the model.** Our unforced Hamiltonian,  $H_{\text{dw}}^\varepsilon \equiv -\partial_x^2 + U_\varepsilon(x)$ , is an asymptotically periodic Schrödinger operator; i.e.,

$$H_{\text{dw}}^\varepsilon = \begin{cases} H_+^\varepsilon & = -\partial_x^2 + V(x) + \varepsilon W(x) \quad \text{for } x \gg +1 \\ H_-^\varepsilon & = -\partial_x^2 + V(x) - \varepsilon W(x) \quad \text{for } x \ll -1, \end{cases}$$

Here,  $H_+^\varepsilon$  and  $H_-^\varepsilon$  are  $\mathbb{Z}-$ periodic. Both  $H_+^\varepsilon$  and  $H_-^\varepsilon$  are perturbations of the underlying bulk operator  $H = -\partial_x^2 + V(x)$ , which has a linear crossing in its band structure at energy  $E_D$  (Dirac point).  $H_\pm^\varepsilon$  have a common spectral gap (called the bulk gap) of width  $\mathcal{O}(\varepsilon)$  about  $E = E_D$ , which is induced by the small but non-compact perturbations  $\pm W(x)$ . The operator  $H_{\text{dw}}^\varepsilon$  interpolates between  $H_-^\varepsilon$  at  $x = -\infty$  and  $H_+^\varepsilon$  at  $x = +\infty$ , via a *domain wall*. It has, for all  $\varepsilon$  small, a protected mid-gap eigenstate  $\psi_\star^\varepsilon(x)$  of energy  $E_D + \mathcal{O}(\varepsilon^2)$ . Moreover,  $\psi_\star^\varepsilon(x)$  has a multi-scale structure; with respect to the band structure of  $H$ , it is (to an excellent approximation) a wave-packet which is spectrally concentrated about the Dirac point with an envelope characterized by the zero energy eigenstate of an effective (homogenized) Dirac operator. A more detailed discussion of the model and its analytic properties is given in Section 3. A realization of this model in photonic waveguides has been studied in [26].

In this article we study the initial value problem for the *parametrically forced Schrödinger equation*

$$i\psi_t = (H_{\text{dw}}^\varepsilon + 2i\varepsilon A(\varepsilon t)\partial_x)\psi, \quad 0 < \varepsilon \ll 1, \quad (1.1)$$

where  $A(T)$  is real-valued and periodic. The perturbing operator  $2i\varepsilon A(\varepsilon t)\partial_x$  arises from a *pseudo-magnetic potential*,  $\varepsilon A(\varepsilon t)$ , induced by a time-dependent deformation of  $H_{\text{dw}}^\varepsilon$ . In Section 1.3, we derive (1.1) in the setting of a coupled array of optical waveguides. This model is also relevant in the context of a coupled array of trapped ultracold fermions [22]. We ask the following:

*Question: Does the topologically protected edge state  $\psi_\star^\varepsilon$  of  $H_{\text{dw}}^\varepsilon$  persist in the presence of time-period forcing ( $A(t) \neq 0$ )?*

## 1.2. Summary of analytical and numerical results.

(A) **Defect mode decay in the Schrödinger equation.** In Figure 1 we contrast the time-evolution (1.1) for the initial data  $\psi(x, 0) = \psi_\star^\varepsilon$ , in the cases

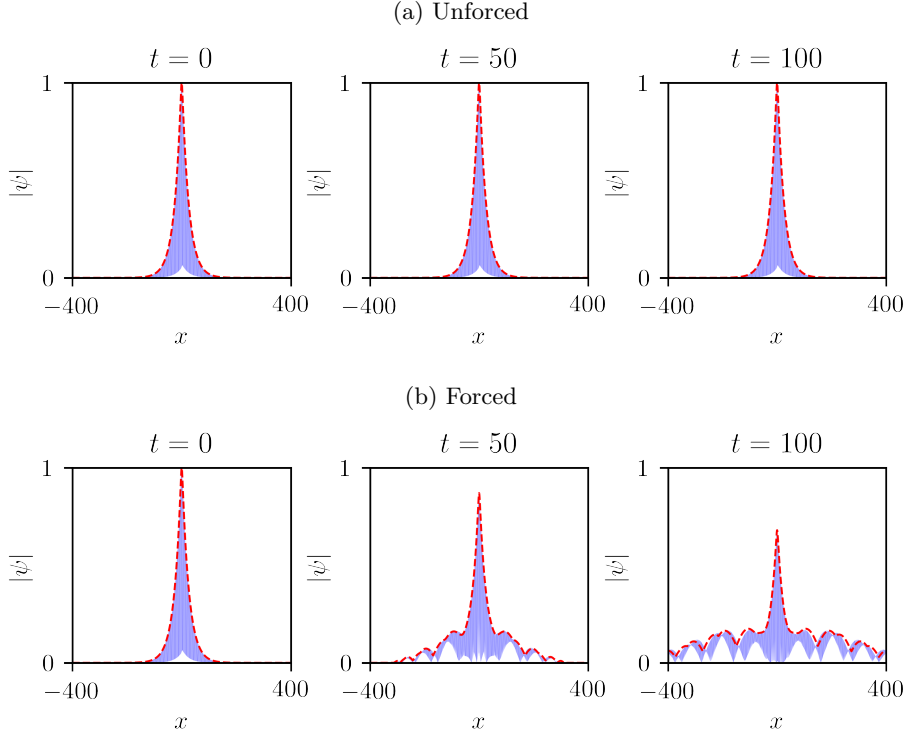


FIGURE 1. (a) Numerically computed evolution of edge state,  $\psi_*^\varepsilon$ , under the unforced Schrödinger equation, (1.1) with  $A(T) \equiv 0$ , (blue, solid) and its envelope evolution approximated by the effective (unforced) Dirac equation (red, dashes). (b) Periodically-forced Schrödinger evolution ( $A(T) \neq 0$ ) and its envelope approximated by an effective periodically-forced Dirac dynamics; see Sections 4 and 6.2.

of unforced ( $A = 0$ ) and forced ( $A \neq 0$ ) dynamics; a detailed discussion is given in Section 4. The top row of Figure 1 is consistent with the persistence of the edge state; indeed, for all  $t$  we have  $\psi(t, x) = e^{-iE_\varepsilon t} \psi_*(x)$ . The slow time-decay of the solution is demonstrated in the bottom row of Figure 1. For a forcing  $\beta A(T) = \beta \cos(\omega T)$  with  $\beta$  small and fixed, the envelope decays at an exponential rate  $\approx \exp(-\beta^2 \varepsilon \Gamma_0 t)$ , for some  $\Gamma_0 = \Gamma_0(\omega) > 0$ . This type of decay is observed only for driving frequencies  $\omega$  above some threshold frequency, which we discuss in item (C) below.

(B) **Effective Dirac equation.** In Section 5 we derive and prove the validity of an effective (spatially homogenized) time-periodically forced Dirac equation (Theorem 5.1 and [37]), as an approximation to the envelope dynamics of forced Schrödinger evolution for initial data which are spectrally localized near the Dirac point. The Dirac dynamics accurately approximate the envelope dynamics for data corresponding to the multiple scale edge state  $\psi_*^\varepsilon(x)$ .

The time-dependent Schrödinger equation (1.1) excites a wide range of spatial and temporal scales. In contrast, the effective Dirac approximation is comparatively easy to solve numerically on long time-scales; its numerical solution does not require the simultaneous resolution of multiple temporal and spatial scales.

A numerical comparison between the Schrödinger equation with  $\psi(0, x) = \psi_*^\varepsilon$  and the effective forced Dirac equation, for data given by the envelope of  $\psi_*^\varepsilon$ , shows excellent agreement on long time scales. In Figure 1 we plot both the numerically computed solution of the (multi-scale) Schrödinger equation (1.1) and the solution of the effective forced Dirac equation. Figure 1 demonstrates that the Schrödinger envelope is very well tracked by the (slowly varying) solution of the effective forced Dirac equation. For nontrivial forcing  $A(T)$ , the envelope-decay in the effective Dirac equation, matches that of the Schrödinger equation on large time-scales.

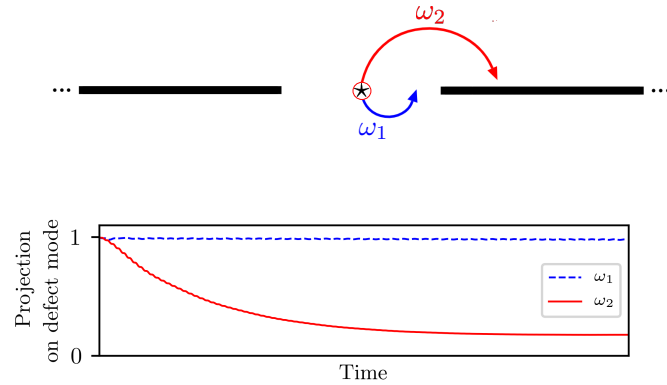


FIGURE 2. **Top:** The spectrum of the unforced Hamiltonian (star and bold lines denote point and continuous spectrum, respectively). **Bottom:** Simulations of the effective forced Dirac equation (5.1), see details in Section 6.2. When the frequency of the forcing is small ( $\omega_1$ , blue dashes), the defect mode does not couple to the continuum modes, and the mode's localization persists. When the frequency is sufficiently large to couple the point and continuous spectrum, i.e.,  $\omega_2 >$  bulk spectral gap, (solid red), power is transferred between the localized mode and the radiation; the defect mode decays.

(C) **Multiscale analysis of radiation damping.** Our results on the approximation of (1.1) by an effective Dirac equation, and an asymptotic solution ( $\beta$  small) of the effective Dirac equation, imply that on large and finite time-scales,  $0 \leq t \leq \varepsilon^{-1}\beta^{-2}$ , the wave-packet decays exponentially

$$\left| \text{Projection of } \psi^\varepsilon(t, \cdot) \text{ on } \psi_*^\varepsilon \right| \approx e^{-\Gamma_0(\omega)\beta^2\varepsilon t}. \quad (1.2)$$

The mechanism of decay is radiation damping; parametric forcing resonantly couples the edge state to radiation modes associated with the continuous spectrum, which acts as an energy sink; see Figure 2. The radiation rate is given by a variant of the *Fermi golden rule*, see, e.g., [38, Chapter 5]. A derivation of this radiation damping effect and, in particular, its rate is given in Section 7. Specifically, we show a threshold effect: if the driving frequency  $\omega$  in the effective Dirac operator is larger than half the spectral gap width, then radiative decay takes place on the time scale  $\beta^{-2}$ .<sup>1</sup>

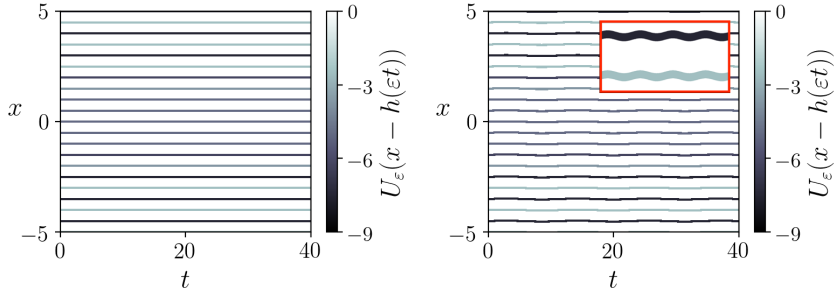


FIGURE 3. **Left:** The domain-wall potential  $U_\varepsilon(x)$ , see (3.4) (in particular  $U_{1/2}^{(2)}$ , see App. B). **Right:** The coiled waveguides potential  $U_\varepsilon(x - h(t))$  with  $h(t) = 2\omega^{-1}\beta \sin(\omega\varepsilon t)$  with a zoom-in in the inset.

**1.3. Derivation of the pseudo-magnetic potential,  $A(T)$ .** We briefly explain how a “pseudo-magnetic potential” in (3.12),  $A(t)$ , arises in the context of nearly monochromatic light-propagation in a planar array of undulating waveguides; see, for example, [1, 2, 23, 31]. Consider a planar array of waveguides, whose index of refraction variations along the transverse ( $x$ ) direction are described by the time-independent potential  $U_\varepsilon(x)$ ; see the left panel of Fig. 3. Illumination of the array on its input side (left) by a continuous wave (CW, nearly monochromatic) laser results in propagation along the longitudinal direction (a time-like direction, labeled  $t$ ) which is approximated by the paraxial Schrödinger equation  $i\psi_t = (-\partial_x^2 + U_\varepsilon)\psi$ . Consider now a planar array of *undulating* waveguides, where the propagation is given by

$$i\partial_t\psi(t, x) = [-\partial_x^2 + U_\varepsilon(x - h(t))] \psi.$$

Here  $h : \mathbb{R} \rightarrow \mathbb{R}$  describes the center-point of waveguides in the array; see right panel of Fig. 3. Switching to the undulating system of coordinates  $\tilde{x} = x - h(t)$ ,  $\tilde{t} = t$ , one gets

$$[i\partial_{\tilde{t}} - ih'(t)\partial_{\tilde{x}}] \psi(\tilde{t}, \tilde{x}) = [-\partial_{\tilde{x}}^2 + U_\varepsilon(\tilde{x})] \psi.$$

Dropping the tilde notation and setting  $h'(t) \equiv 2A(t)$ , we obtain (1.1).

Note that by the further change of variables:  $\phi \equiv \psi \exp(-i \int_0^t |A(s)|^2 ds)$  we obtain a magnetic Schrödinger equation  $i\partial_t\phi = (\partial_x + iA(t))^2\phi + U_\varepsilon(s)\phi$ . By Maxwell’s

<sup>1</sup>If  $\omega$  does not satisfy this resonance condition, then the time scale on which radiative decay takes place is expected to be  $T \approx \beta^{-2r}$ , for some  $r \geq 2$ , with a corresponding result for the Schrödinger evolution.

equations, a spatially-independent magnetic potential  $A(t)$  gives rise to a time-periodic *electric* field and *zero magnetic field*.

#### 1.4. Future directions and open problems.

- **Analytic challenges in rigorously establishing radiative decay.** In our study of the time-decay of defect modes for the effective periodically-forced Dirac Hamiltonian,  $\mathcal{D}(T) = \mathcal{D}_0 + A(T)\sigma_1$ , we derive a formal asymptotic solution, whose validity on the radiation damping time-scale is supported by estimating the expansion terms on the appropriate time-scale. A fully rigorous analysis of this derivation is an open question, which cannot be addressed by an application of previous methods developed in the study of radiative decay in linear and nonlinear radiation damping problems; see, e.g., the time-dependent resonance approach in [7, 28, 39].

We elaborate on the analytic issues. The first challenge arises from the matrix character of the effective Dirac equation; the forcing operator,  $\beta A(T)\sigma_1$ , does not commute with the unperturbed Dirac operator  $\mathcal{D}_0$  and hence cannot be removed via a change of phase. Even if  $\beta$  is assumed to be small, this operator cannot be treated perturbatively; indeed there is no spatial localization in the perturbing operator, which would have allowed for the control of this perturbation via local energy time-decay estimates for  $\exp(-i\mathcal{D}_0 t)$  (on the continuous spectral part of  $\mathcal{D}_0$ ). What could succeed is a variant of the above methods for Floquet Dirac Hamiltonians; in particular, dispersive estimates for forced Dirac Hamiltonians and the necessary spectral decomposition with which to reduce to an appropriate parametrically forced particle-field model (compare with our analysis in Section 8). Research in this direction is currently in progress.

- **Resonant decay in discrete models.** Our study of resonant decay of defect modes is in the context of continuum PDE models. However, the question of existence of Floquet edge modes also appears in the context of discrete (e.g., tight-binding) models in the physics literature [4, 8, 35]. For concreteness, consider the Su-Schrieffer-Heeger (SSH) model, which for a certain parameter regime has a localized edge mode inside a bulk spectral gap. In the numerical investigations of [8], the existence and non-existence of defect modes of time-periodically driven SSH, and the dependence on the driving frequency, is studied. We believe that our approach is applicable to the analysis of such Floquet models.
- **Non-smooth potentials.** Finally we believe that our smoothness assumptions on the coefficients of  $H_{\text{dw}}^\varepsilon$  can be relaxed. However, our discontinuous transition domain wall / dislocation model,  $U_\varepsilon^{(3)}$ , (see Section 4.1 and Appendix B) violates the assumption of a slowly varying domain wall transition. In this case, our the derivation of an effective Dirac operator and hence the asymptotic theory would seem not to apply. Nevertheless, numerical investigation shows that the midgap mode persists and undergoes radiation damping on the time-scale of the previous examples. Furthermore, and remarkably, the damped envelope dynamics are well-described by the effective Dirac operator  $\mathcal{D}^{(3)}(T)$ . It would be of interest to understand this robustness of radiative phenomena against large deformation, i.e., in regimes other than those allowing for a multi-scale structure.

One natural setting to consider would be Schrödinger Hamiltonians, and corresponding effective Dirac Hamiltonians, within the same “topological class”; those which can be continuously deformed into each other without closing the bulk gap. For a study of topological robustness of defect modes against such deformations within a family of dislocation Hamiltonians, see [9].

**1.5. Structure of the paper.** In Section 2 we introduce notation, conventions and briefly review Floquet-Bloch theory for Schrödinger operators on the line with a  $\mathbb{Z}$ -periodic potential. The autonomous Hamiltonian  $H_{\text{dw}}^\varepsilon$  and the parametrically forced Schrödinger equation are discussed in Section 3. Detailed numerical simulations of the parametrically forced Schrödinger equation are presented in Section 4 for concrete choices of domain-wall Schrödinger Hamiltonians. In Section 5 we derive, via a multiple scales analysis, the parametrically forced effective Dirac system and state a theorem on its validity on time-scales of interest. In Section 6 we present results on the radiation damping mechanism in terms of an effective Dirac model, and corroborate our predictions by numerical simulations. The derivation of the radiative decay phenomena is presented in Section 7, and necessary dispersive decay estimates for the unperturbed Dirac operator are derived in Section 8.

**1.6. Acknowledgments.** The authors would like to thank M. Rechtsman and J. Shapiro for stimulating discussions. A.S. acknowledges the support of the AMS-Simons Travel Grant. M.I.W. was supported in part by US National Science Foundation grants DMS-1620418 and DMS-1908657 as well as by the Simons Foundation Math + X Investigator Award #376319.

## 2. PRELIMINARIES

**2.1. Floquet-Bloch theory.** We begin with general remarks on the Floquet-Bloch spectral theory of periodic self-adjoint differential operators; for details, see, e.g., [11, 15, 25, 33]. Let  $V$  be a sufficiently smooth real-valued  $\mathbb{Z}$  periodic potential, i.e.,  $V(x+1) = V(x)$  for all  $x \in \mathbb{R}$ , and introduce the periodic Schrödinger operator

$$H \equiv -\partial_x^2 + V(x), \quad (2.1)$$

acting in the space  $L^2(\mathbb{R})$ .  $H$  is self-adjoint and commutes with translations in the integer lattice,  $\mathbb{Z}$ .

Any  $f \in L^2(\mathbb{R})$  can be represented, via the Floquet-Bloch transform, as a superposition of eigenstates of the integer translation operator  $f(x) \rightarrow f(x+1)$ , i.e.,  $L^2(\mathbb{R}) = \int_{\mathcal{B}}^{\oplus} L_k^2 dk$ , where

$$L_k^2 \equiv \{f \in L_{\text{loc}}^2 : f(x+1; k) = e^{ik} f(x; k)\},$$

where  $k$  varies over  $\mathcal{B} \equiv [0, 2\pi]$ , the fundamental cell of the dual lattice  $2\pi\mathbb{Z}$  (the Brillouin zone). Since  $H$  commutes with integer translations, the spectral theory of  $H$  acting on  $L^2(\mathbb{R})$  can be reduced to the study of  $H$  acting in each  $L_k^2$  space:

$$H = \int_{\mathcal{B}}^{\oplus} H_k dk, \text{ where } H_k = H|_{L_k^2}.$$

For each  $k \in \mathcal{B}$ ,  $H_k$  is a self-adjoint operator and has compact resolvent. Hence, each  $H_k$  has an infinite sequence of finite multiplicity real eigenvalues, tending to infinity

$$E_1(k) \leq E_2(k) \leq \dots \leq E_b(k) \leq \dots .$$

The corresponding eigenmodes (Bloch modes)  $\Phi_b(\cdot; k) \in L_k^2$  satisfy

$$H\Phi_b(x; k) = E_b(k)\Phi_b(x; k), \quad \Phi_b(\cdot; k) \in L_k^2. \quad (2.2)$$

The maps  $E_b : \mathcal{B} \rightarrow \mathbb{R}$  are Lipschitz continuous, and their graphs  $E_b(k)$  are called the *dispersion curves* of  $H$ . The collection of all pairs  $(E_b(k), \Phi_b(x; k))$  for all  $k \in \mathcal{B}$  and  $b \geq 1$  is called the *band structure* of  $H$ .

### 3. HAMILTONIANS; $H_{\text{dw}}^\varepsilon$ AND ITS PERIODIC FORCING, (1.1)

In this section we present a concise systematic discussion (more detailed than in the introduction) of the underlying bulk Hamiltonian,  $H$ , the domain-wall Hamiltonian  $H_{\text{dw}}^\varepsilon$  with asymptotics  $H_\pm^\varepsilon$ , and the parametrically forced Hamiltonian  $H_\varepsilon(t) = H_{\text{dw}}^\varepsilon + 2i\varepsilon\beta A(\varepsilon t)\partial_x$ . Figure 4 will serve as a guide to the hierarchy of time-independent operators and their spectra.

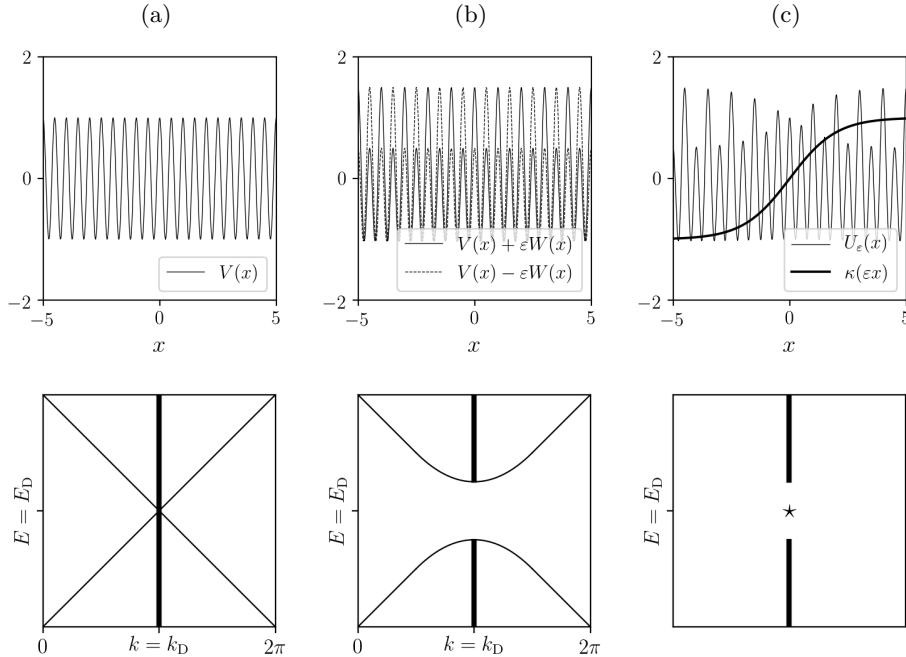


FIGURE 4. Step by step construction of multi-scale domain wall potential  $U_\varepsilon$  (top row) and corresponding spectra (bottom row), following Section 3. **(a)**  $\mathbb{Z}$ -periodic potential,  $V(x)$ , and its linear band-crossing (Dirac point) due to additional  $\frac{1}{2}\mathbb{Z}$ -translation symmetry. **(b)** Perturbed potentials  $V(x) \pm \varepsilon W(x)$  (bulk structure) with minimal period lattice  $\mathbb{Z}$ , and its spectral gap about the Dirac point, due to broken symmetry. **(c)** Asymptotically periodic potential with domain wall defect,  $U_\varepsilon(x)$ ; see (3.4). Interpolating domain wall function  $\kappa(\varepsilon x)$  superimposed. Mid-gap point eigenvalue is indicated. Note that since  $U_\varepsilon$  is not translation invariant,  $k$  is not indicated in the lower panel, just the energy spectrum.

**3.1. Schrödinger Hamiltonians with Dirac points.** We begin with a Schrödinger operator  $H = -\partial_x^2 + V(x)$ , where  $V$  is real-valued and  $\frac{1}{2}\mathbb{Z}$ -periodic, i.e.,  $V(x + \frac{1}{2}) = V(x)$ . For simplicity, we assume that  $V(x)$  is even; for modifications required to treat the general case, see [10]. We shall embed  $H$  in a family of Hamiltonians  $H_\pm^\varepsilon$ , with  $H_\pm^0 = H$  and  $H_\pm^\varepsilon$  of minimal period equal to one. Hence, it is natural to consider  $H$  as acting in  $L^2(\mathbb{R}/\mathbb{Z})$  as having an additional symmetry;  $H$  commutes with  $\frac{1}{2}\mathbb{Z}$  lattice translations.

Due to this additional symmetry, the band structure of  $H$  acting in  $L^2(\mathbb{R}/\mathbb{Z})$  has *Dirac points* [13, 15]: quasi-momentum / energy pairs  $(k_D, E_D)$ , where  $k_D = \pi$ . Specifically, there exists  $b \geq 1$  such that there are dispersion curves  $k \mapsto E_b(k), E_{b+1}(k)$  curves, which cross linearly:

$$E_b(k) - E_D = -v_D |k - k_D| (1 + \mathcal{O}(|k - k_D|)), \quad (3.1a)$$

$$E_{b+1}(k) - E_D = +v_D |k - k_D| (1 + \mathcal{O}(|k - k_D|)), \quad (3.1b)$$

for  $|k - k_D| \ll 1$ , where  $v_D > 0$  is a constant, the Dirac (or Fermi) velocity. The band structure around a Dirac point  $(k, E) = (\pi, E_D)$  is shown in the first column of Figure 4.

It is convenient to introduce a basis  $\{\Phi_1, \Phi_2\}$  of the two-dimensional  $L^2_{k_D}$  eigenspace of  $E_D$ , such that  $\Phi_2(x) = \Phi_1(-x)$ . In terms of this basis

$$v_D \equiv 2i \langle \Phi_1, \partial_x \Phi_1 \rangle_{L^2([0,1])} = -2i \langle \Phi_2, \partial_x \Phi_2 \rangle_{L^2([0,1])}. \quad (3.2)$$

By an appropriate choice of phase of  $\Phi_1$ , one arranges for  $v_D > 0$ .

**3.2. Bulk Hamiltonians  $H_\pm^\varepsilon$ .** Let  $W(x)$  be real-valued and periodic with minimal period 1. We introduce, for  $\varepsilon \neq 0$  and real, bulk operators which break the  $1/2$ -periodicity of  $H$

$$H_\pm^\varepsilon = H \pm \varepsilon W(x), \quad \text{where } W(x + 1/2) = -W(x).$$

Since  $W(x)$  is a non-compact perturbation of  $H$ , it may change the essential spectrum. Indeed, the operators  $H_\pm^\varepsilon$  have a spectral gap about  $E_D$  of width  $\mathcal{O}(\varepsilon)$ ; see [15, Appendix F]. Introducing the shift operator  $S_{\frac{1}{2}}[f](x) \equiv f(x + \frac{1}{2})$ , we have that  $S_{\frac{1}{2}}^* = S_{-\frac{1}{2}}$  and  $S_{\frac{1}{2}} H_+^\varepsilon S_{\frac{1}{2}}^* = H_-^\varepsilon$ . Thus,  $H_+^\varepsilon$  and  $H_-^\varepsilon$  have the same spectrum and, in particular, have a common spectral gap about  $E_D$ . We refer to this common gap as the *bulk spectral gap*.

**3.3.  $H_{\text{dw}}^\varepsilon$ , asymptotically periodic Hamiltonian with domain wall defect.** Introduce a *domain wall function*,  $\kappa(X)$ , which is real-valued and such that

$$\kappa(X) \rightarrow \pm \kappa_\infty \quad \text{as } X \rightarrow \pm \infty, \quad \text{where } \kappa_\infty > 0. \quad (3.3)$$

We then define a *domain wall Hamiltonian* which interpolates between the bulk Hamiltonians  $H_-^\varepsilon$  and  $H_+^\varepsilon$ :<sup>2</sup>

$$H_{\text{dw}}^\varepsilon \equiv -\partial_x^2 + U_\varepsilon(x), \quad U_\varepsilon(x) \equiv V(x) + \varepsilon \kappa(\varepsilon x) W(x), \quad (3.4)$$

Two examples of asymptotically periodic potentials with domain wall defects are displayed in the top and middle panels of Figure 5.

The essential spectrum of  $H_{\text{dw}}^\varepsilon$  is equal to that of the operators  $H_\pm^\varepsilon$ , but point spectrum may arise in the spectral gaps of  $H_{\text{dw}}^\varepsilon$  and, in particular, in the bulk

<sup>2</sup>We take  $V(x)$ ,  $W(x)$  and  $\kappa(x)$  to be sufficiently smooth and  $\kappa^2(X) - \kappa_\infty^2$  tending to zero sufficiently rapidly. Precise smoothness hypotheses on these functions, which we believe can be somewhat relaxed, are spelled out in [15].

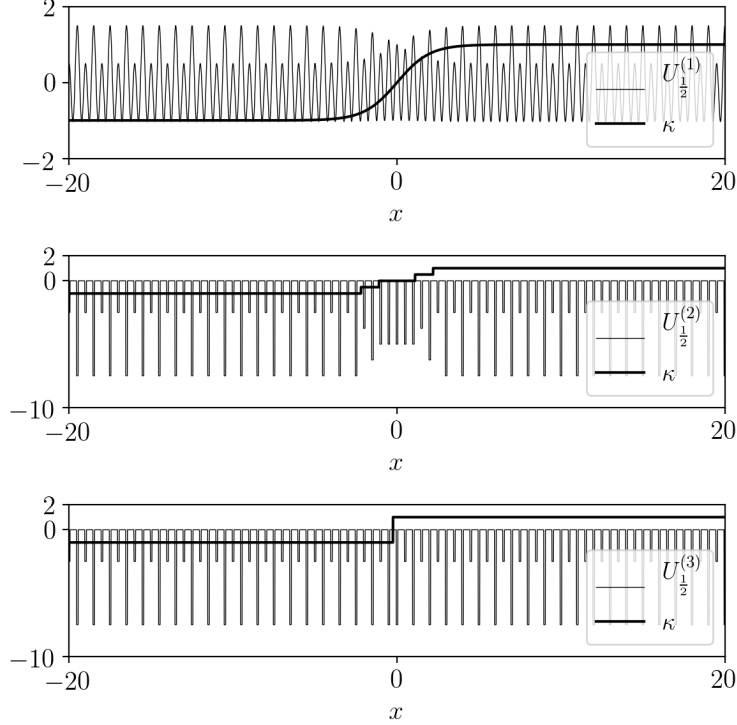


FIGURE 5. Three examples of the potential  $U_\varepsilon$  (3.12) **Top:** Cosine potential (B.1). **Middle:** Periodic array of square-wells (B.4). **Bottom:** Periodic array of square-wells with a sharp transition (B.5).

spectral gap about the Dirac energy  $E_D$ . We next give a brief discussion of the bifurcation of discrete eigenvalues of  $H_{\text{dw}}^\varepsilon$ , from the Dirac point at  $\varepsilon = 0$  into the spectral gap about  $E_D$  for  $\varepsilon$  non-zero and small.

Introduce the effective Dirac operator,  $\not{D}_0$ , defined in terms of the domain wall function  $\kappa(X)$ , Dirac velocity  $v_D$ , and  $\vartheta_\sharp \equiv \langle \Phi_1, W\Phi_2 \rangle$ :

$$\not{D}_0 \equiv iv_D\sigma_3\partial_X + \vartheta_\sharp\kappa(X)\sigma_1, \quad (3.5)$$

where the Pauli matrices are

$$\sigma_1 = \begin{pmatrix} 0 & 1 \\ 1 & 0 \end{pmatrix}, \quad \sigma_2 = \begin{pmatrix} 0 & -i \\ i & 0 \end{pmatrix}, \quad \sigma_3 = \begin{pmatrix} 1 & 0 \\ 0 & -1 \end{pmatrix}. \quad (3.6)$$

Note that the parameters  $v_D$  and  $\vartheta_\sharp$  are determined by the ‘‘Dirac eigenspace’’ for the energy  $E_D$ . Since  $\kappa(X) \rightarrow \pm\kappa_\infty$  as  $X \rightarrow \pm\infty$ , the continuum spectrum of  $\not{D}_0$  acting in  $L^2(\mathbb{R}; \mathbb{C}^2)$  is equal to  $(-\infty, -|\vartheta_\sharp|\kappa_\infty] \cup [|\vartheta_\sharp|\kappa_\infty, \infty)$ .

The spectrum of  $\not{D}_0$  also contains a discrete eigenvalue at zero energy,  $\alpha_*(X)$ , satisfying:

$$\not{D}_0\alpha_* = 0, \quad \|\alpha_*\|_{L^2(\mathbb{R})} = 1$$

It is easily verified that  $\alpha_*$  is given, up to a constant phase, by

$$\alpha_*(X) = C \left( \frac{1}{i} \right) e^{-(\vartheta_{\sharp}/v_D) \int_0^X \kappa(s) ds}, \quad (3.7)$$

where  $C > 0$  is a normalization constant. Since  $\kappa_{\infty} > 0$ , the function (3.7) is exponentially decaying at infinity. Thus it is the change in sign of  $\kappa(X)$  that is responsible for the existence of a robust zero energy eigenstate; zero is a rigid eigenvalue with respect to perturbations which of  $\kappa(X)$  which are spatially localized.

To simplify the discussion, we make the

$$\text{Assumption: } 0 \text{ is the only eigenvalue of } \mathcal{D}_0. \quad (3.8)$$

Its corresponding normalized eigenstate is denoted  $\alpha_*$ :

$$\mathcal{D}_0 \alpha_* = 0, \quad \|\alpha_*\|_{L^2(\mathbb{R})} = 1.$$

This assumption is satisfied, for example, by  $\mathcal{D}_0$  for  $\kappa(X) = \tanh(X)$ ; see [27, Appendix A]. A schematic of the spectrum of  $\mathcal{D}_0$  is shown in Figure 6.

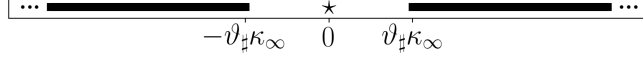


FIGURE 6. Spectrum of the (unforced) Dirac operator  $\mathcal{D}_0$ , see (3.5).

The defect mode  $\alpha_*$  of the Dirac equation (3.5) seeds a corresponding defect mode of the Schrödinger equation (3.4):

**Theorem 3.1** (Theorem 5.1 in [15]; see also [10,13]). *There exists  $\varepsilon_0 > 0$  such that for all  $0 < |\varepsilon| < \varepsilon_0$ , the following is a characterization of all point spectrum in the spectral gap about  $E_D$ , bounded away from the edges of the continuous spectrum:*

(1) *There exists a smooth curve defined for  $\varepsilon \in [0, \varepsilon_0]$ :*

$$\begin{aligned} \varepsilon &\mapsto E^{\varepsilon} = E_D + \mathcal{O}(\varepsilon^2) \in (E_D - |\vartheta_{\sharp}| \kappa_{\infty} \varepsilon, E_D + |\vartheta_{\sharp}| \kappa_{\infty} \varepsilon), \\ \varepsilon &\mapsto \psi_*^{\varepsilon} \in H^1(\mathbb{R}) \end{aligned}$$

*such that  $(E^{\varepsilon}, \psi_*^{\varepsilon})$  is a normalized eigenpair of  $H_{\text{dw}}^{\varepsilon}$*

$$H_{\text{dw}}^{\varepsilon} \psi_*^{\varepsilon} = E^{\varepsilon} \psi_*^{\varepsilon}. \quad (3.9)$$

(2) *The eigenstate  $\psi_*^{\varepsilon}$  has a multi-scale structure; to leading order in  $\varepsilon$ , it is a Dirac wave packet, a slow modulation of the two-dimensional eigenspace  $\text{span}\{\Phi_1, \Phi_2\}$ , associated with the Dirac point at  $(k, E) = (\pi, E_D)$  (see Section 3.1):*

$$\begin{aligned} \psi_*^{\varepsilon}(x) &= \varepsilon^{\frac{1}{2}} \left( \alpha_{*,1}(\varepsilon x) \Phi_1(x; k_D) + \alpha_{*,2}(\varepsilon x) \Phi_2(x; k_D) \right) + \mathcal{O}_{H^2(\mathbb{R})}(\varepsilon) \\ &\equiv \varepsilon^{\frac{1}{2}} \alpha_*(\varepsilon x)^{\top} \Phi(x) + \mathcal{O}_{H^2(\mathbb{R})}(\varepsilon). \end{aligned} \quad (3.10)$$

*The envelope,  $\alpha_*(X) = (\alpha_{1*}(X), \alpha_{2*}(X))^{\top}$ , is given by (3.7), the zero energy eigenstate of the effective Dirac operator  $\mathcal{D}_0$ .*

In Appendix A we present a derivation of effective Dirac equation in the more general (temporally-forced) setting of (1.1); see also [15,37]. Two examples of defect states  $\psi_*^{\varepsilon}(x)$  and the corresponding envelopes  $\alpha_*(X)$  are displayed in Figure 7.

*Remark 3.2.* We may relax the assumption (3.8). In general  $\mathcal{D}_0$  has  $2N + 1$  of eigenvalues in its bulk gap  $(-|\vartheta_\sharp|\kappa_\infty, +|\vartheta_\sharp|\kappa_\infty)$  for some  $N \geq 0$ : a zero energy eigenvalue, (3.7), and  $2N$  eigenvalues located symmetrically about zero. In [10], a more general version of Theorem 3.1 is proved in which the point spectrum of  $H_{\text{dw}}^\varepsilon$  is given by  $2N+1$  eigenvalues in its  $\mathcal{O}(\varepsilon)$  width spectral gap about  $E_D$ , with analogous multiple scale expansions of the corresponding edge eigenstates. We believe that the results of this article (numerical and analytical) on radiation damping can be extended to this multimode setting; see [24] for relevant analysis.

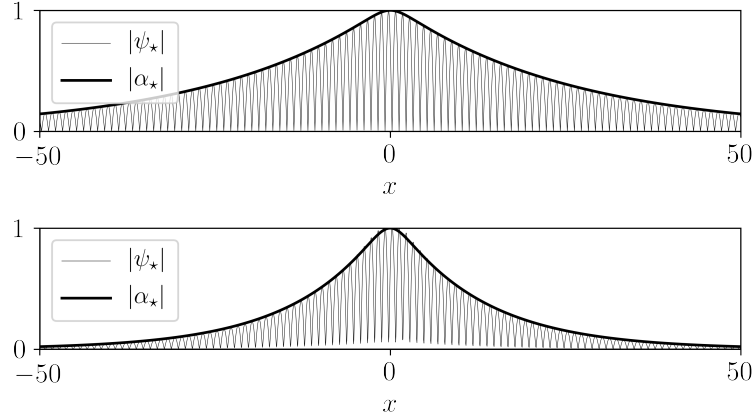


FIGURE 7. The amplitude of  $|\psi_\star^\varepsilon|$ , the defect mode of the Schrödinger Hamiltonian  $H_{\text{dw}}^\varepsilon$  (3.9), grey), showing its multi-scale (carrier + envelope) structure for (a)  $U_\varepsilon^{(1)}$  (B.1), and (b)  $U_\varepsilon^{(2)}$  (B.4), see also Figure 5. The envelope is well-approximated by  $\alpha_\star$ , ((3.8), black), of the corresponding Dirac operator  $\mathcal{D}_0$ , see (3.5).

**3.4. Floquet model; parametric time-periodic forcing of  $H_{\text{dw}}^\varepsilon$ .** Our goal in this paper is to study the effect of time-periodic (parametric) forcing on the defect state  $\psi_\star$  of  $H_{\text{dw}}^\varepsilon$ ; see (3.4) and (3.10). Denote our time-periodic Hamiltonian by

$$H_\varepsilon(t) \equiv H_{\text{dw}}^\varepsilon + 2i\varepsilon\beta A(\varepsilon t)\partial_x = -\partial_x^2 + U_\varepsilon(x) + 2i\varepsilon\beta A(\varepsilon t)\partial_x \quad (3.11)$$

where  $A(T)$  is  $T_{\text{per}} = 2\pi/\omega$ -periodic. We shall study the initial value problem:

$$i\partial_t\psi(t, x) = H_\varepsilon(t)\psi, \quad (3.12a)$$

$$\psi(0, x) = \psi_\star^\varepsilon(x). \quad (3.12b)$$

In Section 4, we present long-time numerical simulations of (3.12) showing the resonant radiation damping effect, and in Sections 5 and 6, we provide an analytical understanding of this phenomenon on the physically interesting time-scale.

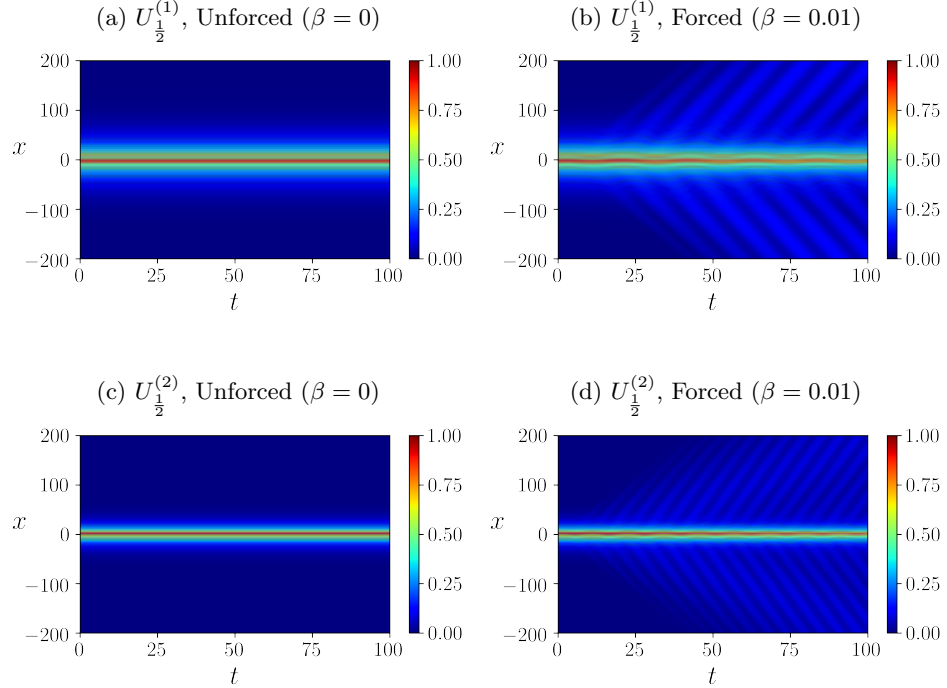


FIGURE 8. Solutions of (3.12) with  $\psi(0, x) = \psi_*(x)$ . **(a)**  $U_{\frac{1}{2}}^{(1)}$  with  $\beta = 0$ , the unforced problem, and **(b)** with  $\beta = 0.01$  and  $\omega = 0.6$ . **(c)** and **(d)** Same as (a) and (b), respectively, for  $U_{\frac{1}{2}}^{(2)}$  with  $\omega = 1.1$ .

#### 4. LONG-TIME SIMULATIONS OF THE FORCED SCHRÖDINGER EQUATION, (3.12); SLOW RADIATIVE DECAY OF THE DEFECT STATE

In this section we numerically investigate the long-time behavior of solutions of the initial value problem (3.12) for two Hamiltonians:

$$H_\varepsilon^{(\ell)}(t) = -\partial_x^2 + U_\varepsilon^{(\ell)}(x) + 2i\varepsilon\beta \cos(\varepsilon\omega t)\partial_x, \quad \ell = 1, 2, \quad (4.1)$$

- (1)  $U_\varepsilon^{(1)}$  smoothly interpolates between asymptotic phase shifted cosine-potentials
- (2)  $U_\varepsilon^{(2)}$  interpolates between asymptotic phase-shifted arrays of double square wells

for different choices of the parameters  $\beta, \omega > 0$ . See the top two panels of Figure 5 for illustrations of  $U_\varepsilon^{(1)}$  and  $U_\varepsilon^{(2)}$ . Throughout our simulations, we set  $\varepsilon = 1/2$ . The precise definitions of  $U_\varepsilon^{(j)}$  are given in Appendix B. Details concerning the numerical method are given in Appendix C.

Consider first the case  $\beta = 0$ . Defect-mode initial data  $\psi(x, 0) = \psi_*(x)$  gives rise to the solution  $\psi(t, x) = e^{-iE_\varepsilon t}\psi_*(x)$ ; see (3.9). Figures 8a and 8c indeed show, for both potential choices, that  $|\psi(t, x)| = |\psi_*(x)|$  for  $0 \leq t \leq 100$ .

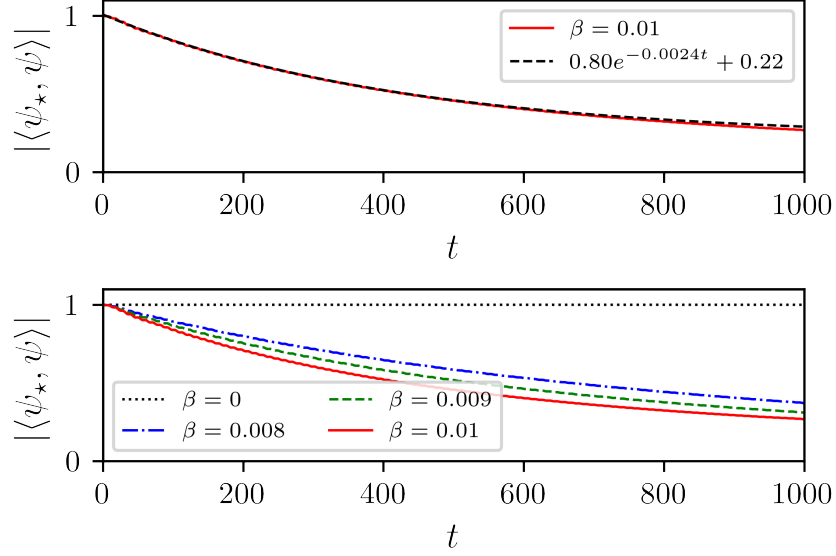


FIGURE 9. Projections of solutions of (3.12) with  $U_\varepsilon^{(1)}$ ,  $\omega = 0.6$ , and  $\psi(0, x) = \psi_*(x)$  onto  $\psi_*(x)$ . **Top:** An exponential decay fitted to the projection for  $\beta = 0.01$ . The projection curve and the fitted line are nearly indistinguishable. **Bottom:** The projection  $|\langle \psi_*, \psi(t, \cdot) \rangle_{L^2(\mathbb{R})}|$  for  $\beta = 0, 0.008, 0.009, 0.01$ .

We next consider the dynamics *under temporal forcing*. For  $U_\varepsilon^{(1)}$  (and  $U_\varepsilon^{(2)}$ ) we fix  $\omega = 0.6$  (and  $\omega = 1.1$ , respectively) and  $\beta > 0$  and observe decay of the solution with advancing time; see Figs. 8b and 8d.<sup>3</sup>

In Fig. 9, we explore the decay rate by tracking the time-dependence of projection of the solution,  $\psi(\cdot, t)$ , onto the defect state, i.e.,  $\langle \psi_*, \psi(t, \cdot) \rangle_{L^2(\mathbb{R})}$ . Our numerical results ( $U_\varepsilon^{(1)}$  with  $\varepsilon = 1/2$ ) are consistent with exponential decay of this projection over the very long time scale,  $t \leq 1000$ ,  $\langle \psi_*, \psi(t, \cdot) \rangle_{L^2(\mathbb{R})} \approx \exp(-\Gamma t)$ . Further, we studied the dependence of the exponential rate,  $\Gamma$ , on  $\beta$  over a range of small  $\beta$ . The decay is consistent with a decay  $\sim \exp(-\Gamma(\beta)t)$ , where  $\Gamma(\beta) \sim \beta^{2.07}$  and  $\sim \beta^{2.10}$  for  $U_\varepsilon^{(1)}$  and  $U_\varepsilon^{(2)}$ , respectively.

**4.1. The case of a sharp transition.** In the potential  $U_\varepsilon^{(2)}$ , the transition between the asymptotics at  $-\infty$  and  $+\infty$  is done *slowly* via a piecewise constant domain wall function  $\kappa(X)$ . A more common configuration in optical experiments is a sharp transition between phase-shifted waveguide arrays [5]; see lower panel of Figure 5.

Thus we consider (4.1) with  $U_\varepsilon^{(3)}$ , where the asymptotic bulk potentials,  $V(x) \pm \varepsilon W(x)$ , are identical to those of  $U_\varepsilon^{(2)}$  (see Appendix B), but now  $\kappa(X) = \text{sgn}(X)$ .

<sup>3</sup>The choice of  $\omega = 1.1$  in Fig. 8d is not an arbitrary one. In Section 6 we show that radiation damping to occurs if  $|\omega|$  exceeds half the bulk spectral gap width of  $\mathcal{D}_0$ , the effective Dirac Hamiltonian, see Fig. 2. For  $U_\varepsilon^{(1)}$ , which is derived from  $U_\varepsilon^{(1)}$ , the size of the bulk spectral gap is 1, and therefore  $|\omega| > 0.5$  satisfies the resonance condition (similarly with  $|\omega| > 1$  for  $U_\varepsilon^{(2)}$ ).

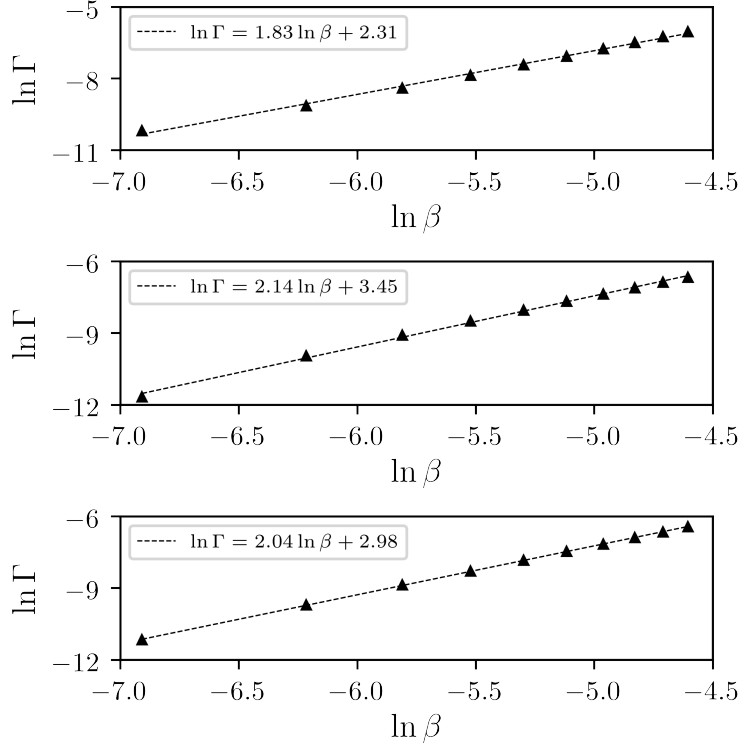


**FIGURE 10. Top:** The decay rate  $\Gamma$  against the forcing amplitude  $\beta$  on a log-log scale (triangles) and an exponential fit of  $\Gamma \sim \beta^{1.83}$ . **Middle and Bottom:** Same as the first row, for  $U_\varepsilon^{(2)}$  and  $U_\varepsilon^{(3)}$  respectively, with  $\omega = 1.1$ , and exponential fits of  $\Gamma \sim \beta^{2.14}$  and  $\Gamma \sim \beta^{2.04}$ .

Due to the very different scaling properties of  $U_\varepsilon^{(3)}$ , the analysis leading to Theorem 3.1 does not apply. However, we expect similar qualitative behavior.

We repeated our simulations for  $U_\varepsilon^{(3)}$  and have corroborated these heuristics. We observe, as in the previous examples, that  $H_{\text{dw}}^\varepsilon$  has a defect mode which, under periodic forcing, radiation damps on time scales of order  $\beta^{-2}$ ; see Figure 10.

## 5. THE EFFECTIVE DIRAC EQUATION

Our goal in this section is to approximate the multi-scale evolution of the Schrödinger equation (3.12) by a simpler effective envelope dynamics. The separation of fast scales ( $x$  and  $t$ ) of the underlying Bloch modes and slow scales ( $X = \varepsilon x$  and  $T = \varepsilon t$ ) of the domain wall and parametric forcing, allow for the derivation of an effective homogenized equation for wave-packet envelope.

In Appendix A we show that the envelope of the solution of the time-periodically forced initial value problem (3.12), with initial data

$$\psi(0, x) = \psi_\star^\varepsilon(x) \approx \varepsilon^{1/2} \alpha_\star(\varepsilon x)^\top \Phi(x)$$

evolves in the form

$$\psi(t, x) \approx \varepsilon^{\frac{1}{2}} \alpha(\varepsilon t, \varepsilon x)^\top \Phi(x) e^{-iE_D t}$$

where  $\alpha(T, X)$  is governed by the initial value problem for an effective periodically-forced Dirac equation:

$$i\partial_T \alpha(T, X) = \not{D}(T)\alpha, \quad \alpha(0, X) = \alpha_0(X) \in H^4(\mathbb{R}; \mathbb{C}^2). \quad (5.1a)$$

$$\not{D}(T) \equiv \not{D}_0 + v_D A(T) \sigma_3, \quad (5.1b)$$

Here,  $\not{D}_0$  is given by (3.5) and the Pauli matrices  $\sigma_1$  and  $\sigma_3$ , see (3.6).

Let  $\psi_0 \mapsto \mathcal{U}^\varepsilon[\psi_0](t, x)$  denote the solution of Schrödinger equation (3.12) with  $\psi(0, \cdot) = \psi_0$ , and  $\alpha_0(X) \mapsto \mathcal{U}_{\text{Dir}}[\alpha_0](T, X)$  denote the solution of the effective Dirac equation (5.1) with  $\alpha(0, \cdot) = \alpha_0$ .

**Theorem 5.1** (Effective Dirac dynamics). *There exists  $\varepsilon_0 > 0$  such that for all  $0 < \varepsilon < \varepsilon_0$ , the following holds: Consider (3.12), the Schrödinger equation with time periodic Hamiltonian, and initial data of the form,  $\psi_0(x) = \varepsilon^{1/2} \alpha_0(\varepsilon x)^\top \Phi(x)$ , with  $\alpha_0 \in H^4(\mathbb{R}^2; \mathbb{C}^2)$ . Fix constants  $T_0 > 0$  and  $0 < \rho < 1$ .*

*Then, there is a constant,  $C$ , which depends on the Hamiltonian  $H$ ,  $\rho$  and  $\alpha_0$ , such that for  $0 \leq t \leq T_0 \varepsilon^{-(2-\rho)}$ ,*

$$\left\| \mathcal{U}^\varepsilon[\psi_0](t, x) - \varepsilon^{\frac{1}{2}} \mathcal{U}_{\text{Dir}}[\alpha_0](\varepsilon t, \varepsilon x)^\top \Phi(x; k_D) e^{-iE_D t} \right\|_{L^2(\mathbb{R}_x)} \leq C \varepsilon^\rho. \quad (5.2)$$

Analogous results on the effective Dirac dynamics in two-dimensional analogs of (3.12), unforced and forced, were obtained in [14, 37]. Theorem 5.1 follows from arguments which closely follow those in [37, Section 8].

## 6. METASTABILITY OF EDGE STATES AND RADIATION DAMPING

In Section 6.1 we summarize our analytical results on radiation damping for initial value problem for the periodically forced (magnetic) Dirac equation:

$$i\partial_T \alpha = (\not{D}_0 + \beta A(T) \sigma_3) \alpha, \quad \alpha(0, X) = \alpha_*(X). \quad (6.1)$$

Here,

- (1)  $A(T)$  is  $T_{\text{per}}$ -periodic and of mean zero
- (2)  $\not{D}_0 = i\sigma_3 \partial_X + \kappa(X) \sigma_1$ , and
- (3)  $\alpha_*$  is the zero-energy defect mode of  $\not{D}_0$ :

$$\not{D}_0 \alpha_* = 0, \quad \|\alpha_*\|_{L^2(\mathbb{R})} = 1.$$

The parameter  $\beta$ , the strength of periodic forcing, is taken to be small.

After discussing our results for the forced Dirac initial value problem (6.1), we apply them to radiation damping in the initial value problem for the forced Schrödinger equation. In Section 6.2 we present numerical simulations which corroborate our theoretical predictions. The multiscale analysis underlying the results in Section 6.1 is presented in Section 7.

**6.1. Summary of analytical results on radiation damping.** For  $\beta = 0$ , the solution of (7.1) is  $\alpha(T, X) = \alpha_*(X)$  for all  $T \in \mathbb{R}$ .

For  $\beta$  small, it is natural to represent the solution to the perturbed evolution equation (7.1) using the spectral theory of the operator  $\not{D}_0$ , outlined in Section 3.3. In particular, for the case that  $\not{D}_0$  has only bound state we have:

$$\text{spec}(\not{D}_0) = \{0\} \cup \mathbb{R} \setminus [-\vartheta_\# \kappa_\infty, \vartheta_\# \kappa_\infty].$$

The  $L^2(\mathbb{R}; \mathbb{C}^2)$ -orthogonal projections onto the bound (defect) state subspace and the continuous (dispersive) spectral subspace of  $\mathcal{D}_0$  are, respectively:

$$\mathcal{P}_0 = \langle \alpha_\star, \cdot \rangle \alpha_\star \quad \text{and} \quad \mathcal{P}_c = I - \mathcal{P}_0 \quad (\mathcal{P}_0 + \mathcal{P}_c = I). \quad (6.2)$$

Thus, we decompose the solution of (5.1) relative to these orthogonal projections:

$$\alpha(T, X) = g(T)\alpha_\star(X) + \alpha_d(T, X), \quad \langle \alpha_\star(\cdot), \alpha_d(T, \cdot) \rangle = 0, \quad T \geq 0, \quad (6.3)$$

In Section 7 we derive a coupled dynamical system for the oscillator-like degree of freedom,  $g(T; \beta)$  and field-like degree of freedom  $\alpha_d(T, X; \beta)$ , which we solve for small  $\beta$  via a multiple scale expansion. Our constructed  $g(T)$  decays on the time scale  $\mathcal{O}(\beta^{-2})$ . In particular, we show the following:

**Leading order multiscale expansion:** Fix  $T_0 > 0$  and arbitrary. Then, there exist  $\rho_0, \beta_0 > 0$  such that for all  $0 < \beta < \beta_0$  and  $0 \leq T \leq T_0\beta^{-2}$

$$g(T; \beta) = e^{i(\beta\eta_A(T) + \beta^2\Lambda_0)T} e^{-\Gamma_0\beta^2T} (1 + o(1)) \quad (6.4a)$$

$$\alpha_d(T, X) = \mathcal{O}(\beta e^{-\Gamma_0\beta^2T}) \quad \text{in } L^2(\langle x \rangle^{-\rho_0} dx), \quad \text{as } \beta \rightarrow 0. \quad (6.4b)$$

Here,  $\Gamma_0 = \Gamma_0(\omega)$  is given by

$$\Gamma_0(\omega) \equiv \frac{\pi}{4} \left\langle \mathcal{P}_c \sigma_3 \alpha_\star, (\delta(\mathcal{D}_0 + \omega) + \delta(\mathcal{D}_0 - \omega)) \mathcal{P}_c \sigma_3 \alpha_\star \right\rangle \geq 0, \quad (6.5)$$

is generically *strictly positive*,

$$\Lambda_0(\omega) \equiv \frac{1}{4} \left\langle \mathcal{P}_c \sigma_3 \alpha_\star, \left( \text{PV} \frac{1}{\mathcal{D}_0 + \omega} + \text{PV} \frac{1}{\mathcal{D}_0 - \omega} \right) \mathcal{P}_c \sigma_3 \alpha_\star \right\rangle, \quad (6.6)$$

and

$$\eta_A(T) = \langle \alpha_\star, \sigma_3 \alpha_\star \rangle \int_0^T A(s) ds$$

is a real, bounded, and  $T_{\text{per}}$ -periodic.

**Exponential decay on the time scale  $\mathcal{O}(\beta^{-2})$ :** Note from (6.4) that exponential decay on the time-scale  $T \sim \beta^{-2}$  holds if  $\Gamma_0(\omega) > 0$ . Since  $\delta(\mathcal{D}_0 \pm \omega)$  are non-negative self-adjoint operators,  $\Gamma_0(\omega) \geq 0$  for any  $\omega$ . The vector  $\delta(\mathcal{D}_0 \pm \omega) \mathcal{P}_c \sigma_3 \alpha_\star$  is the projection of vector  $\mathcal{P}_c \sigma_3 \alpha_\star$  onto the continuous spectral subspace of  $\mathcal{D}_0$  at frequency  $\mp \omega$ . Hence, if  $|\omega| < \kappa_\infty |\vartheta_\sharp|$ , i.e.,  $\omega$  is in the spectral gap of  $\mathcal{D}_0$ , then  $\Gamma_0(\omega) = 0$ , see Fig. 11.

On the other hand, suppose  $|\omega| > \kappa_\infty |\vartheta_\sharp|$ , then  $\omega$  is in the continuous spectrum of  $\mathcal{D}_0$ . For generic data,  $\delta(\mathcal{D}_0 \pm \omega) \mathcal{P}_c \sigma_3 \alpha_\star$  is non-zero, as we expect generic functions to have non-zero projection on every part of the continuous spectrum [3, Section 4]. Hence, generically  $\Gamma_0 > 0$  implying exponential decay.

Since  $\mathcal{P}_c \sigma_3 \alpha_\star \in L^2(\mathbb{R}; \mathbb{C}^2)$ , the inner product (6.5) which gives the exponential rate of decrease,  $\Gamma_0(\omega)$ , decays to zero for  $|\omega| \rightarrow \infty$ . Our numerical simulations in the bottom row of Figure 11 are consistent with this behavior; we observe that  $\omega \mapsto g(T; \omega)|_{T=500}$  increases for  $\omega$  sufficiently large, consistent with rate of decay of  $g(T; \omega)$  being slower for large  $|\omega|$ .

*Remark 6.1.* We expect that the exponential decay is a large-time transient, which applies on the time scale  $T \lesssim \beta^{-2}$ . While our analysis does not cover  $|T| \gg \beta^{-2}$ , we expect the time-decay to be algebraic and given by the free dispersive rate,  $\mathcal{O}(t^{-1/2})$ ; see, e.g., [39].

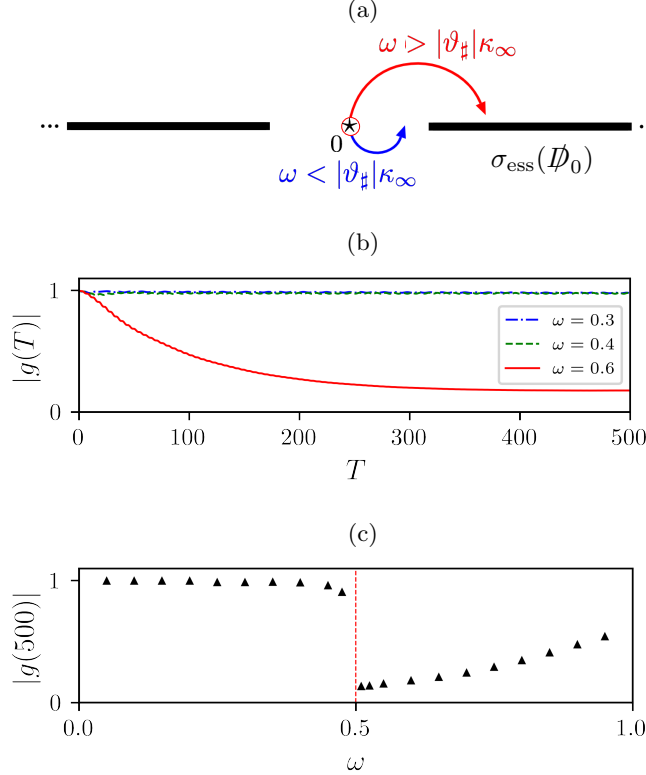


FIGURE 11. The effect of the frequency  $\omega$  of the forcing  $A(T)$  on the decay of the Dirac zero mode  $\alpha_*$ , see (3.8). (a) When  $|\omega| > |\vartheta_\sharp| \kappa_\infty$  (red),  $\alpha_*$  couples to the essential spectrum. Otherwise  $|\omega| < |\vartheta_\sharp| \kappa_\infty$  (blue), and the coupling effect is expected to be negligible. (b) Same settings as in Fig. 1a, where  $\vartheta_\sharp \kappa_\infty = 0.5$ . The projection onto the zero mode  $g(T) = \langle \alpha_*, \alpha(\cdot, T) \rangle_{L^2(\mathbb{R}; \mathbb{C}^2)}$  for  $\beta = 0.01$ , with  $\omega \in \{0.3, 0.4, 0.6\}$ . The curves for  $\omega = 0.3$  and  $\omega = 0.4$  are nearly indistinguishable. (c)  $g(500)$  for varying values of  $\omega$  (triangles) and a dotted line for the  $\omega = \vartheta_\sharp \kappa_\infty$  threshold.

#### Radiative time-decay in parametrically forced Schrödinger equation:

In terms of the original variables of the parametrically forced Schrödinger equation (3.12) we have, by (6.4a), for  $\rho \in (0, 1)$  and  $0 \leq t \leq T_0 \varepsilon^{-(2-\rho)}$ ,

$$\langle \psi_*, \psi(t, \cdot) \rangle_{L^2(\mathbb{R})} = e^{-i\beta \eta_A(\varepsilon t)} e^{-iE^\varepsilon t} e^{-\beta^2 \varepsilon (\Gamma_0 + i\Lambda_0)t} + \mathcal{O}(\beta, \varepsilon^\rho),$$

and where  $E^\varepsilon = E_D + \mathcal{O}(\varepsilon^2)$ ; see (3.9). This gives exponential decay on the time-scale  $\mathcal{O}(\varepsilon^{-1} \beta^{-2})$ .

**6.2. Simulations of the effective Dirac equation.** For the time-periodically forced Schrödinger equations (3.12) with the potentials  $U_\varepsilon^{(l)}$  ( $l = 1, 2, 3$ ), introduced in Section 4, we consider the effective periodically-forced Dirac Hamiltonians

$$\mathcal{D}^{(l)}(T) = \mathcal{D}_0^{(l)} + v_D A(T) \sigma_3 \quad (l = 1, 2, 3);$$

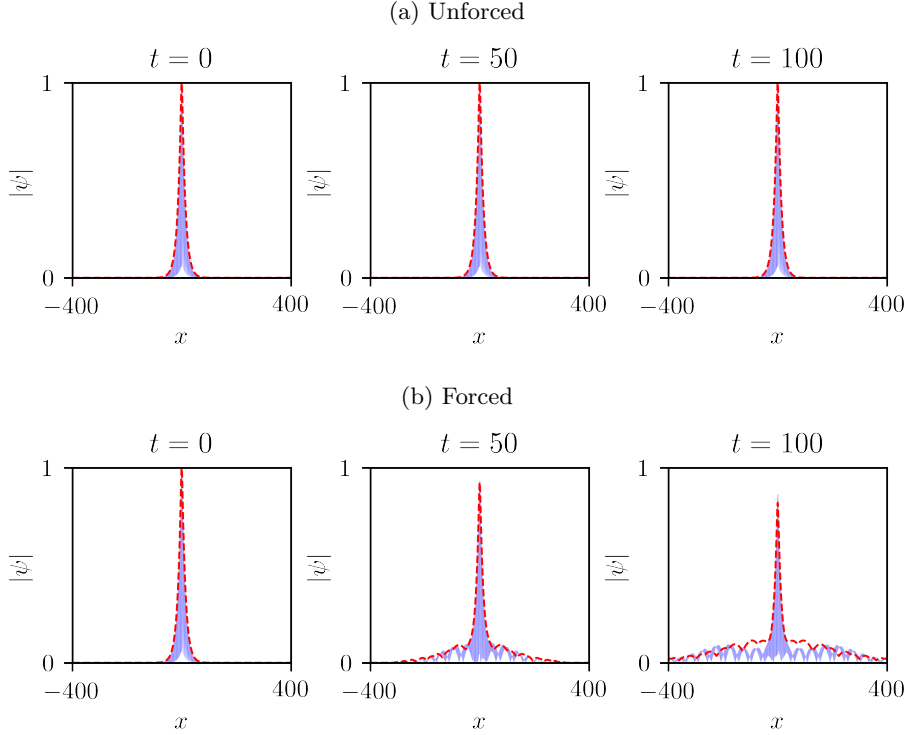


FIGURE 12. Same as Fig. 1, only for the square well Schrödinger and Dirac equations, (B.4) and (B.8), respectively, with  $\omega = 1.1$ .

see (5.1b). The parameters which define these effective operators are given in Appendix B.

To confirm the analytical asymptotic results outlined in Section 6.1, we simulate the evolution under the effective Hamiltonians  $\mathcal{D}^{(1)}(T)$  (Fig. 1) and  $\mathcal{D}^{(2)}(T)$  (Fig. 12), and compare the solution  $\alpha(T, X)$  with the wave-envelope of the solution of the corresponding Schrödinger equations (3.12) with  $\varepsilon = 1/2$ . In the unforced case ( $\beta = 0$ ), the envelope of the Schrödinger defect mode  $|\psi_*(x)|$  is tracked very well by  $|\alpha_*(\varepsilon x)|$  for  $0 \leq t \leq 100$ , as we expect from (3.10).<sup>4</sup> For the forced cases, we see that the Dirac envelope decays and fits the multi-scale Schrödinger solution extremely well for  $t = 50$ , and quite well (though small discrepancies do appear) up to  $t = 100$ .

Figure 13 presents numerical results on radiation damping rate for the effective Dirac Hamiltonians  $\mathcal{D}^{(\ell)}(T)$ ,  $(\ell = 1, 2, 3)$  which are consistent with the predicted exponential decay rate,  $\Gamma(\beta) = \Gamma_0 \beta^2$ , (see (6.4a)). These results are almost one-to-one comparable with those of the corresponding Schrödinger equations; compare with Figure 10.

<sup>4</sup>Note that, since  $\varepsilon = 1/2$  in (3.12), the simulation of (5.1) runs on the slow time-scale of  $0 \leq T \leq 50$ .

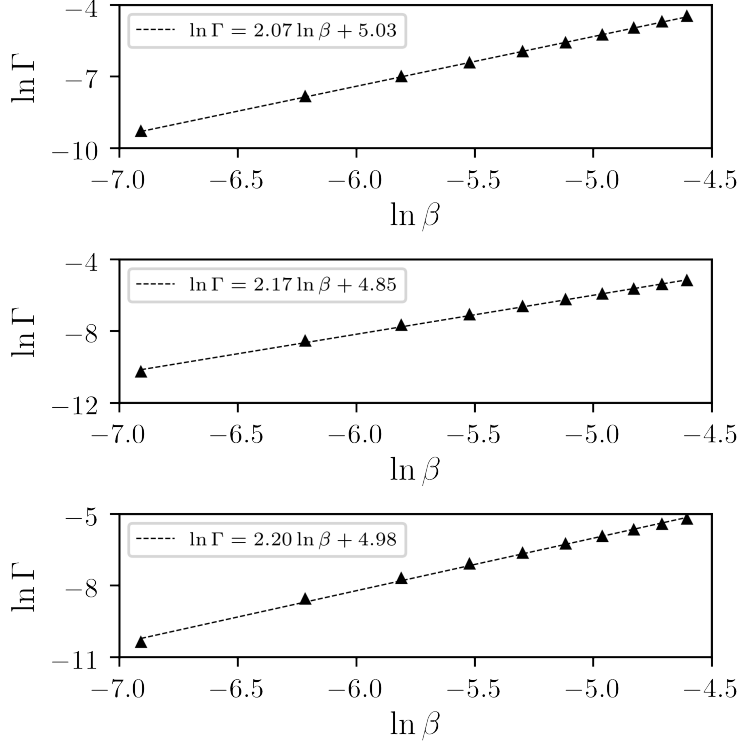


FIGURE 13. Decay rates for the effective Dirac equations as a function of  $\beta$ , see (5.1). **Top:**  $\mathcal{D}_0^{(1)}$ . **Middle:**  $\mathcal{D}_0^{(2)}$ . **Bottom:**  $\mathcal{D}_0^{(3)}$ .

It is remarkable that the effective dynamics given by  $\mathcal{D}^{(3)}(T)$  (with a discontinuous  $\kappa(X)$ ) tracks the Schrödinger dynamics for large time, since the Hamiltonian violates the scaling assumptions used to derive the effective Dirac dynamics from the Schrödinger dynamics. We remarked on this as an open problem in Section 1.4.

## 7. MULTISCALE ANALYSIS OF RADIATION DAMPING

In this section, we provide a multiple scale analysis and derivation of the radiation damping phenomena observed in our numerical simulations. Consider the initial-value-problem (IVP) for  $\alpha(T, X)$ , the effective parametrically forced Dirac equation (5.1) with initial data given by the zero energy defect mode,  $\alpha_*(X)$ , of the unforced Dirac operator  $\mathcal{D}_0$ :

$$i\partial_T \alpha = (\mathcal{D}_0 + \beta A(T)\sigma_3)\alpha, \quad \alpha(0, X) = \alpha_*(X). \quad (7.1)$$

In (7.1) we have inserted a parameter,  $\beta$ , multiplying the forcing function,  $A(T)$ ;  $\beta$  is real and will be taken sufficiently small. Recall that since  $\alpha_*$  is the zero energy eigenstate of  $\mathcal{D}_0$ , we have that if  $\beta = 0$ , then  $\alpha(T, X) = \alpha_*(X)$ .

Since  $\beta$  is small it is natural to decompose  $\alpha$  into its projection onto the bound state and the dispersive part of  $\mathcal{D}_0$ , orthogonal to  $\alpha_*$

$$\alpha(T, X) = g(T)\alpha_*(X) + \alpha_d(T, X), \quad \langle \alpha_*(\cdot), \alpha_d(T, \cdot) \rangle = 0; \quad (7.2)$$

see also (6.3).

Inserting (6.3) into (5.1), and using the relation  $\mathcal{D}_0\alpha_* = 0$ , we obtain<sup>5</sup>

$$i\partial_T g(T)\alpha_* + i\partial_T\alpha_d(T) = \mathcal{D}_0\alpha_d(T) + \beta v_D A(T)g(T)\sigma_3\alpha_* + \beta v_D A(T)\sigma_3\alpha_d(T). \quad (7.3)$$

Applying the projections  $\mathcal{P}_0$  and  $\mathcal{P}_c$ , as defined in (6.2), to (7.3), we obtain the coupled system for  $g(T)$  and  $\alpha_d(T)$ :

$$i\partial_T g(T) = \beta\langle\alpha_*, \sigma_3\alpha_*\rangle A(T)g(T) + \beta A(t)\langle\alpha_*, \sigma_3\alpha_d(T)\rangle, \quad (7.4)$$

$$i\partial_T\alpha_d(T) = \mathcal{D}_0\alpha_d(T) + \beta\mathcal{P}_c\sigma_3\alpha_* A(T)g(T) + \beta A(T)\mathcal{P}_c\sigma_3\alpha_d(T), \quad (7.5)$$

$$g(0) = 1, \quad \alpha_d(0) = 0. \quad (7.6)$$

To avoid cumbersome expressions, we have set  $\vartheta_\sharp = v_D = 1$ . The first term on the right hand side of (7.4) contributes a rapidly varying phase, which we can remove by setting

$$G(T) \equiv e^{i\beta\eta_A(T)}g(T), \quad \text{where} \\ \eta_A(T) \equiv \langle\alpha_*, \sigma_3\alpha_*\rangle \int_0^T A(s) ds. \quad (7.7)$$

Note that since  $A(T)$  has mean zero,<sup>6</sup>  $\eta_A(T)$  is bounded on  $\mathbb{R}$ . Equations (7.4), (7.5), (7.6) becomes a system for  $G(T)$  and  $\alpha_d(T)$ :

$$i\partial_T G(T) = \beta e^{i\beta\eta_A(T)} A(T) \langle\alpha_*, \sigma_3\alpha_d(T)\rangle, \quad (7.8a)$$

$$(i\partial_T - \mathcal{D}_0) \alpha_d(T) = \beta \mathcal{P}_c\sigma_3\alpha_* e^{-i\beta\eta_A(T)} A(T) G(T) + \beta \mathcal{P}_c\sigma_3 A(T) \alpha_d(T). \quad (7.8b)$$

$$G(0) = 1, \quad \alpha_d(0) = 0. \quad (7.8c)$$

The structure of (7.8) and numerical simulations (Section 6.2) suggest that solution varies on disparate temporal scales: from the rapid time-scale of order  $\beta^0 = 1$ , of the forcing function,  $A(T)$ , to the decay time-scale of the bound state amplitude,  $\beta^{-2}$ . Thus, we shall seek the solution of (7.8) in the form of a multiple scale expansion. First, introduce the hierarchy of time scales

$$T, \quad \tau_1 = \beta T, \quad \tau_2 = \beta^2 T, \quad (\beta \text{ small})$$

and view  $G$  and  $\alpha_d$  as functions of these variables. Thus, (7.8) becomes:

$$i(\partial_T + \beta\partial_{\tau_1} + \beta^2\partial_{\tau_2})G(T, \tau_1, \tau_2) = \beta e^{i\beta\eta_A(T)} A(T) \langle\alpha_*, \sigma_3\alpha_d(T, \tau_1, \tau_2)\rangle, \quad (7.9a)$$

$$i(\partial_T + \beta\partial_{\tau_1} + \beta^2\partial_{\tau_2})\alpha_d(T, \tau_1, \tau_2) - \mathcal{D}_0\alpha_d(T, \tau_1, \tau_2) \\ = \beta \mathcal{P}_c\sigma_3\alpha_* e^{-i\beta\eta_A(T)} A(T) G(T, \tau_1, \tau_2) + \beta \mathcal{P}_c\sigma_3 A(T) \alpha_d(T, \tau_1, \tau_2). \quad (7.9b)$$

Next, we expand the solution  $(G(\cdot; \beta), \alpha_d(\cdot; \beta))$  of (7.9) in the small parameter  $\beta$ :

$$G = G^{(0)} + \beta G^{(1)} + \beta^2 G^{(2)} + \dots, \quad G^{(n)}(T, \tau_1, \tau_2) \in \mathbb{C}, \quad (7.10a)$$

$$\alpha_d = \alpha_d^{(0)} + \beta\alpha_d^{(1)} + \beta^2\alpha_d^{(2)} + \dots, \quad \alpha_d^{(n)}(T, \tau_1, \tau_2) \perp \alpha_*. \quad (7.10b)$$

<sup>5</sup>In the calculations below, we shall frequently suppress the  $X$ -dependence of  $\alpha_d$ . Thus,  $\alpha(T) = g(T)\alpha_* + \alpha_d(T)$ .

<sup>6</sup>Without loss of generality, we can assume  $A(T)$  has mean zero. Otherwise, the mean of  $A(T)$  can be removed by a change of variables.

We capture the initial data (7.8c) by imposing the initial conditions:

$$G^{(0)} = 1, \quad \text{for } T = 0, \tau_1 = 0, \tau_2 = 0, \quad (7.11a)$$

$$G^{(n)} = 0 \quad \text{for } T = 0, \tau_1 = 0, \tau_2 = 0 \text{ and all } n \geq 1, \quad (7.11b)$$

$$\alpha^{(n)} = 0 \quad \text{for } T = 0, \tau_1 = 0, \tau_2 = 0 \text{ and all } n \geq 1. \quad (7.11c)$$

Substitution of (7.10) into (7.9) and equating like terms in powers of  $\beta$ , leads to a hierarchy of equations for the functions  $\{G^{(n)}\}_{n \geq 0}$  and  $\{\alpha^{(n)}\}_{n \geq 0}$ . These functions are determined by the requirement that contributions from terms at one order in  $\beta$  are smaller or equal to terms of lower order in  $\beta$  on the radiation damping time-scale  $T \sim \beta^{-2}$ .

For any fixed  $\hat{T} > 0$  and  $n \geq 1$ , we require that:

$$\lim_{\beta \downarrow 0} \sup_{0 \leq T \leq \hat{T}/\beta^2} \beta^n |G^{(n)}(T, \beta T, \beta^2 T)| = 0, \quad (7.12)$$

$$\lim_{\beta \downarrow 0} \sup_{0 \leq T \leq \hat{T}/\beta^2} \beta^n \|\langle X \rangle^{-\rho} \alpha^{(n)}(T, \beta T, \beta^2 T, X)\|_{L^2(\mathbb{R}_X)} = 0. \quad (7.13)$$

Here,  $\rho > 0$  is fixed and is taken sufficiently large.

The norm in (7.13) is a measure of spatially localized energy and below we see how it naturally arises. We shall construct the order  $\beta^0$ ,  $\beta^1$  and  $\beta^2$  terms of the expansion (7.9) in order to exhibit the transient exponential decay on the time-scale  $T \sim \beta^{-2}$ . The expansion can be carried out systematically to any finite order in  $\beta$ . Section 7.1 assembles some technical tools used along the way and the expansion is constructed in Section 7.2.

**7.1. Technical interlude.** Throughout this section, assume that  $\kappa_\infty = 1$ , i.e., that  $\lim_{X \rightarrow \pm\infty} \kappa(X) = \pm 1$ , and furthermore, that the convergence to  $\pm 1$  is sufficiently fast.<sup>7</sup> We shall also assume that  $\kappa(X)$  is smooth. While such assumptions are stringent, our numerical simulations in Sections 4 and 6.2 suggest that the phenomena is not dependent on such smoothness properties.

For any  $\epsilon > 0$ , we the operator  $e^{-i\mathcal{D}_0 s}/(\mathcal{D}_0 - \lambda + i\epsilon)$  is bounded in  $L^2(\mathbb{R})$ . Introduce the operator

$$\frac{e^{-i\mathcal{D}_0 s}}{(\mathcal{D}_0 - \lambda + i0)} \equiv \lim_{\epsilon \rightarrow 0^+} \frac{e^{-i\mathcal{D}_0 s}}{(\mathcal{D}_0 - \lambda + i\epsilon)}. \quad (7.14)$$

**Proposition 7.1.** *For any  $r \geq r_0 > 0$  sufficiently large, there exist  $\rho > 0$  such that Assume  $\lambda \in \text{spec}_{\text{ess}}(\mathcal{D}_0)$  but that  $\lambda$  is not an endpoint of  $\text{spec}_{\text{ess}}(\mathcal{D}_0)$ . The operator  $e^{-i\mathcal{D}_0 s}(\mathcal{D}_0 - \lambda + i0)^{-1}$  is well-defined from  $L^2(\langle x \rangle^r dx)$  to  $L^2(\langle x \rangle^{-r} dx)$  and satisfies the following local energy decay bound for all  $t > 0$ :*

$$\left\| \langle x \rangle^{-r} \frac{e^{-i\mathcal{D}_0 s}}{(\mathcal{D}_0 - \lambda + i0)} \langle x \rangle^{-r} \right\|_{\mathcal{B}(L^2)} \leq C \langle t \rangle^{-\rho}, \quad .$$

See Section 8 for the proof of Proposition 7.1.

<sup>7</sup>A sufficient condition for the decay rate of  $\kappa(X)$  emerges from our application of wave operators in Section 8.2; see [42, 43].

**Proposition 7.2.** (1) For  $f \in \mathcal{S}(\mathbb{R})$ , the following identity holds in  $L^2(\langle x \rangle^{-\rho} dx)$  for a fixed  $\rho > 0$ :

$$\int_0^s e^{-i\mathcal{D}_0(s-s_1)} A(s_1) \mathcal{P}_c f_1 \, ds_1 = \mathcal{G}(s) \mathcal{P}_c f \quad (7.15)$$

Here,  $\mathcal{G}(t)$  denotes the operator

$$\mathcal{G}(s) = \frac{1}{2i} e^{i\omega s} \text{PV} \frac{1}{\mathcal{D}_0 + \omega} \mathcal{P}_c + \frac{1}{2i} e^{-i\omega s} \text{PV} \frac{1}{\mathcal{D}_0 - \omega} \mathcal{P}_c \quad (7.16a)$$

$$+ \frac{\pi}{2} (e^{i\omega s} \delta(\mathcal{D}_0 + \omega) + e^{-i\omega s} \delta(\mathcal{D}_0 - \omega)) \mathcal{P}_c \quad (7.16b)$$

$$- \frac{e^{-i\mathcal{D}_0 s}}{i(\mathcal{D}_0 + \omega + i0)} \mathcal{P}_c - \frac{e^{-i\mathcal{D}_0 s}}{i(\mathcal{D}_0 - \omega + i0)} \mathcal{P}_c. \quad (7.16c)$$

(2) For  $f_1, f_2 \in \mathcal{S}(\mathbb{R})$ ,

$$\left\langle \mathcal{P}_c f_2, \int_0^s e^{-i\mathcal{D}_0(s-s_1)} A(s_1) \mathcal{P}_c f_1 \, ds_1 \right\rangle = \langle \mathcal{P}_c f_1, \mathcal{G}(s) \mathcal{P}_c f_2 \rangle. \quad (7.17)$$

(3) For  $f \in \mathcal{S}(\mathbb{R})$ , we have  $\sup_{s \geq 0} \|\langle x \rangle^{-\rho} \mathcal{G}(s) f\|_{L^2} < \infty$ .

*Proof of Proposition 7.2.* The lemma is a consequence of the following calculation which holds in  $\mathcal{S}'(\mathbb{R})$ . For any fixed  $s \geq 0$ , we compute evaluate the integral via a regularization procedure. Using that  $A(s) = \cos(\omega s)$  we have :

$$\begin{aligned} \int_0^s e^{-i\mathcal{D}_0(s-s')} A(s') \mathcal{P}_c \, ds' &= \frac{1}{2} \int_0^s e^{-i\mathcal{D}_0 s} (e^{i(\mathcal{D}_0 + \omega)s'} + e^{i(\mathcal{D}_0 - \omega)s'}) \mathcal{P}_c \, ds' \\ &= \lim_{\epsilon \rightarrow 0^+} \frac{1}{2} \int_0^s e^{-i\mathcal{D}_0 s} (e^{i(D_0 + \omega + i\epsilon)s'} + e^{i(\mathcal{D}_0 - \omega + i\epsilon)s'}) \mathcal{P}_c \, ds' \\ &= \frac{1}{2} \lim_{\epsilon \rightarrow 0^+} \left[ \frac{e^{i\omega s} - e^{-i\mathcal{D}_0 s}}{i(\mathcal{D}_0 + \omega + i\epsilon)} + \frac{e^{-i\omega s} - e^{-i\mathcal{D}_0 s}}{i(\mathcal{D}_0 - \omega + i\epsilon)} \right] \mathcal{P}_c \end{aligned}$$

Recall the distributional identity (Plemelj-Sokhotski relation)

$$\frac{1}{x - i0} = \lim_{\epsilon \rightarrow 0^+} \frac{1}{x - i\epsilon} = \text{PV} \frac{1}{x} + i\pi \delta(x) \quad (7.18)$$

where PV denotes the Cauchy Principal Value. Applying (7.18) we obtain

$$\int_0^s e^{-i\mathcal{D}_0(s-s')} A(s') \mathcal{P}_c \, ds' = \mathcal{G}(s).$$

Here,  $\mathcal{G}(s)$  is displayed in (1). Finally, to prove the uniform bound in item (3), we return to the decomposition of  $\mathcal{G}(s)$  as given in (1). That the operators in (7.16c) satisfy the desired bound is a direct result of Proposition 7.1. The other terms (7.16a)–(7.16b), can be written (and are obtained from) as  $e^{\pm i\omega s} [\mathcal{D}_0 \pm \omega]^{-1}$ . The required bound can be reduced to the analogous bounds for  $e^{\pm i\omega s} [Z_0 \pm \omega]^{-1}$ , where  $Z_0$  is the free Schrödinger Hamiltonian. The details of a similar argument are presented in Section 8, and in particular Section 8.2.

□

**7.2. Implementing the expansion through order  $\beta^2$ .** We wish to substitute (7.10) into (7.9) and equate terms of like power in  $\beta$  leads to a hierarchy of equations for the functions  $G^{(n)}$  and  $\alpha^{(n)}$ . The only non-algebraic term,  $e^{i\beta_A(T)}$ , is expanded to

$$e^{i\beta\eta_A(T)} = 1 + i\beta\eta_A(T) + \mathcal{O}(\beta^2).$$

By recalling that  $\eta_A(T)$  is bounded, we obtain the hierarchy equations, the first several of which we now display and solve.

**$\mathcal{O}(\beta^0)$  equation.**

$$i\partial_T G^{(0)} = 0, \quad (i\partial_T - \mathcal{D}_0)\alpha^{(0)} = 0 \quad (7.19)$$

**$\mathcal{O}(\beta^1)$  equation.**

$$i\partial_T G^{(1)} = -i\partial_{\tau_1} G^{(0)} + A(T) \left\langle \sigma_3 \alpha_{\star}, \alpha^{(0)} \right\rangle \quad (7.20a)$$

$$(i\partial_T - \mathcal{D}_0)\alpha^{(1)} = -i\partial_{\tau_1} \alpha^{(0)} + \mathcal{P}_c \sigma_3 \alpha_{\star} A(T) G^{(0)} + \mathcal{P}_c \sigma_3 \alpha_{\star} A(T) \alpha^{(0)}. \quad (7.20b)$$

**$\mathcal{O}(\beta^2)$  equation.**

$$\begin{aligned} i\partial_T G^{(2)} = & -i\partial_{\tau_1} G_1 - i\partial_{\tau_2} G^{(0)} + A(T) \left\langle \sigma_3 \alpha_{\star}, \alpha^{(1)} \right\rangle \\ & + i\eta_A(T) \left\langle \sigma_3 \alpha_{\star}, \alpha^{(0)} \right\rangle \end{aligned} \quad (7.21a)$$

$$\begin{aligned} (i\partial_T - \mathcal{D}_0)\alpha^{(2)} = & -i\partial_{\tau_1} \alpha^{(1)} - i\partial_{\tau_2} \alpha^{(0)} + \mathcal{P}_c \sigma_3 \alpha_{\star} \eta_A(T) A(T) G^{(0)} \\ & + \mathcal{P}_c \sigma_3 \alpha_{\star} A(T) \alpha^{(1)}. \end{aligned} \quad (7.21b)$$

.....

**$\mathcal{O}(\beta^n)$  :** .....

We next solve the equations of this hierarchy through order  $\beta^2$ .

**$\mathcal{O}(\beta^0)$  solution.** Since  $i\partial_T G^{(0)} = 0$ , we have that

$$G^{(0)} = G^{(0)}(\tau_1, \tau_2) \quad (7.22)$$

Furthermore,  $(i\partial_T - \mathcal{D}_0)\alpha^{(0)} = 0$  with initial data  $\alpha^{(0)}(0) = 0$  implies that we can take

$$\alpha^{(0)}(T) \equiv 0. \quad (7.23)$$

**$\mathcal{O}(\beta^1)$  solution.** Using that  $\alpha^{(0)}(T) \equiv 0$ , the next order of equations simplifies to

$$i\partial_T G^{(1)} = -i\partial_{\tau_1} G^{(0)}, \quad (7.24)$$

$$(i\partial_T - \mathcal{D}_0) \alpha^{(1)} = \mathcal{P}_c \sigma_3 \alpha_* A(T) G^{(0)}. \quad (7.25)$$

Integrating (7.24) and using that  $G^{(1)}$  vanishes for  $T = 0$ , we have

$$iG^{(1)}(T, \tau_1, \tau_2) = -i\partial_{\tau_1} G^{(0)}(\tau_1, \tau_2)T.$$

Condition (7.12) for  $n = 1$  then implies  $\partial_{\tau_1} G^{(0)}(\tau_1, \tau_2) = 0$  and hence  $i\partial_T G^{(1)} = 0$ . Therefore,

$$G^{(0)} = G^{(0)}(\tau_2) \quad \text{and} \quad G^{(1)} = G^{(1)}(\tau_1, \tau_2).$$

The degrees of freedom offered by  $G^{(1)}(\tau_1, \tau_2)$  are not required to remove resonances in subsequent terms of the hierarchy; we however need to satisfy (7.11b) for  $n = 1$ . We can therefore set

$$G^{(1)} \equiv 0. \quad (7.26)$$

We solve (7.25) using Duhamel's principle and obtain, using Proposition 7.2, that

$$\begin{aligned} \alpha^{(1)}(T, \tau_2) &= -i \int_0^T e^{-i\mathcal{D}_0(T-s)} \mathcal{P}_c \sigma_3 \alpha_* A(s) ds G^{(0)}(\tau_2) \\ &= \mathcal{G}(T) \mathcal{P}_c \sigma_3 \alpha_* G^{(0)}(\tau_2). \end{aligned} \quad (7.27)$$

Hence, by item (3) of Proposition 7.2, for  $\rho$  taken sufficiently large we have

$$\| \langle X \rangle^{-\rho} \alpha^{(1)}(T, X, \tau_2) \|_{L^2(\mathbb{R}_X)} \lesssim |G^{(0)}(\tau_2)|, \quad \text{for } T \geq 0. \quad (7.28)$$

Below we determine  $G^{(0)}(\tau_2) = G^{(0)}(\beta^2 T)$ , which we shall see is bounded for on the time scale  $\beta^{-2}$ . Therefore, by (7.28), (7.13) is satisfied for  $n = 1$ .

**$\mathcal{O}(\beta^2)$  solution.** The system (7.21) reduces to

$$i\partial_T G^{(2)} = -i\partial_{\tau_2} G^{(0)} + A(T) \left\langle \sigma_3 \alpha_*, \alpha^{(1)}(T, \tau_2) \right\rangle \quad (7.29a)$$

$$(i\partial_T - \mathcal{D}_0) \alpha^{(2)} = \mathcal{P}_c \sigma_3 \alpha_* \eta_A(T) A(T) G^{(0)} + \mathcal{P}_c \sigma_3 \alpha_* A(T) \alpha^{(1)}. \quad (7.29b)$$

Integration of (7.29a), using the initial condition  $G^{(2)}(0) = 0$ , implies

$$iG^{(2)}(T, \tau_2) = T \left( -i\partial_{\tau_2} G^{(0)}(\tau_2) + \frac{1}{T} \int_0^T A(s) \left\langle \sigma_3 \alpha_*, \alpha^{(1)}(s, \tau_2) \right\rangle ds \right) \quad (7.30)$$

Since we seek an expansion where, in particular,  $\sup_{0 \leq T \leq \beta^{-2}} \beta^2 |G^{(2)}(T)| = o(1)$  as  $\beta \downarrow 0$ , we require that

$$i\partial_{\tau_2} G^{(0)}(\tau_2) = \lim_{T \rightarrow \infty} \frac{1}{T} \int_0^T A(s) \left\langle \sigma_3 \alpha_*, \alpha^{(1)}(s, \tau_2) \right\rangle ds. \quad (7.31)$$

Let's next study the inner product:  $\left\langle \sigma_3 \alpha_*, \alpha^{(1)}(s, \tau_2) \right\rangle$  appearing in (7.31). By (7.27),

$$\begin{aligned} &\left\langle \sigma_3 \alpha_*, \alpha^{(1)}(s, \tau_2) \right\rangle \\ &= -i \left\langle \sigma_3 \alpha_*, \int_0^s e^{-i\mathcal{D}_0(s-s')} A(s_1) \mathcal{P}_c \sigma_3 \alpha_* ds' \right\rangle G^{(0)}(\tau_2) \end{aligned}$$

Therefore,  $G^{(0)}(\tau_2)$  satisfies:

$$i\partial_{\tau_2}G^{(0)}(\tau_2) = \lim_{T \rightarrow \infty} \frac{1}{T} \int_0^T \Upsilon(s) A(s) ds \, G^{(0)}(\tau_2), \quad (7.32)$$

where

$$\Upsilon(s) = -i \left\langle \sigma_3 \alpha_{\star}, \int_0^s e^{-i\mathcal{D}_0(s-s')} A(s_1) \mathcal{P}_c \sigma_3 \alpha_{\star} ds' \right\rangle \quad (7.33)$$

In order to evaluate the limit in (7.32), we apply Proposition 7.2 with  $f_1 = f_2 = \sigma_3 \alpha_{\star}$  to expand the expression for  $\Upsilon(s)$

$$\begin{aligned} \Upsilon(s) &= -i \left\langle \mathcal{P}_c \sigma_3 \alpha_{\star}, \int_0^s e^{-i\mathcal{D}_0(s-s_1)} A(s_1) \mathcal{P}_c \sigma_3 \alpha_{\star} ds_1 \right\rangle \\ &= -\frac{e^{i\omega s}}{2} \left\langle \mathcal{P}_c \sigma_3 \alpha_{\star}, \text{PV} \frac{1}{\mathcal{D}_0 + \omega} \mathcal{P}_c \sigma_3 \alpha_{\star} \right\rangle - \frac{e^{-i\omega s}}{2} \left\langle \mathcal{P}_c \sigma_3 \alpha_{\star}, \text{PV} \frac{1}{\mathcal{D}_0 - \omega} \mathcal{P}_c \sigma_3 \alpha_{\star} \right\rangle \\ &\quad - \frac{i\pi}{2} e^{i\omega s} \langle \mathcal{P}_c \sigma_3 \alpha_{\star}, \delta(\mathcal{D}_0 + \omega) \mathcal{P}_c \sigma_3 \alpha_{\star} \rangle - \frac{i\pi}{2} e^{-i\omega s} \langle \mathcal{P}_c \sigma_3 \alpha_{\star}, \delta(\mathcal{D}_0 - \omega) \mathcal{P}_c \sigma_3 \alpha_{\star} \rangle \\ &\quad + \Upsilon_1(s). \end{aligned}$$

The first four terms in  $\Upsilon(s)$  lead to the resonant decay formulas (6.5)–(6.6). The error term,  $\Upsilon_1(s)$ , is given by:

$$\Upsilon_1(s) \equiv \left\langle \mathcal{P}_c \sigma_3 \alpha_{\star}, \left( \frac{e^{-i\mathcal{D}_0 s}}{i(\mathcal{D}_0 + \omega + i0)} + \frac{e^{-i\mathcal{D}_0 s}}{i(\mathcal{D}_0 - \omega + i0)} \right) \mathcal{P}_c \sigma_3 \alpha_{\star} \right\rangle,$$

and will now be shown to decay with  $s$ .

Since  $\alpha_{\star}$  is exponentially decaying, for any fixed  $r > 0$  we have

$$|\Upsilon_1(t)| \leq \left\| \langle x \rangle^r \sigma_3 \alpha_{\star} \right\|_{L^2} \cdot \sum_{\pm} \left\| \langle x \rangle^{-r} \frac{e^{-i\mathcal{D}_0 t}}{i(\mathcal{D}_0 \pm \omega + i0)} \mathcal{P}_c \sigma_3 \alpha_{\star} \right\|_{L^2}. \quad (7.35)$$

By Proposition 7.1 we have  $\alpha_{\star}$  is exponentially decaying, and thus there exists  $r > 0$  such that

$$|\Upsilon_1(s)| \lesssim \langle s \rangle^{-\rho}, \quad \text{with } \rho > 0. \quad (7.36)$$

Next, substituting  $A(s) = \cos(\omega s) = (e^{i\omega s} + e^{-i\omega s})/2$  into (7.34) and using the bound (7.36) we obtain

$$\lim_{T \rightarrow \infty} \frac{1}{T} \int_0^T A(s) \Upsilon(s) ds = -\Gamma_0 + i\Lambda_0, \quad (7.37)$$

where

$$\Gamma_0 = -\frac{i\pi}{4} (\langle \mathcal{P}_c \sigma_3 \alpha_{\star}, \delta(\mathcal{D}_0 + \omega) \mathcal{P}_c \sigma_3 \alpha_{\star} \rangle + \langle \mathcal{P}_c \sigma_3 \alpha_{\star}, \delta(\mathcal{D}_0 - \omega) \mathcal{P}_c \sigma_3 \alpha_{\star} \rangle) \quad (7.38)$$

$$\Lambda_0 = -\frac{1}{4} \left( \left\langle \mathcal{P}_c \sigma_3 \alpha_{\star}, \text{PV} \frac{1}{\mathcal{D}_0 + \omega} \mathcal{P}_c \sigma_3 \alpha_{\star} \right\rangle + \left\langle \mathcal{P}_c \sigma_3 \alpha_{\star}, \text{PV} \frac{1}{\mathcal{D}_0 - \omega} \mathcal{P}_c \sigma_3 \alpha_{\star} \right\rangle \right) \quad (7.39)$$

Equation (7.32) and (7.37) imply

$$\partial_{\tau_2} G^{(0)}(\tau_2) = (-\Gamma_0 + i\Lambda_0) G^{(0)}(\tau_2). \quad (7.40)$$

The operators  $\delta(\mathcal{D}_0 \pm \omega)$  are non-negative self-adjoint operators. Generically, since  $\omega \in \text{spec}_{ess}(\mathcal{D}_0)$ ,  $\Gamma$  is strictly positive [3, Section 4] and hence  $G^{(0)}(\tau_2)$  is exponentially decaying. Since  $\tau_2 = \beta^2 T$ , the decay is on the time scale  $T \sim \beta^{-2}$ .

Returning now to the expression for  $G^{(2)}(\tau_2)$  in (7.30) we have

$$G^{(2)}(T, \tau_2) = -T \left( \frac{1}{T} \int_0^T A(s) \Upsilon(s) \, ds - (-\Gamma_0 + i\Lambda_0) \right) G^{(0)}(\tau_2), \quad (7.41)$$

where, by (7.37), the expression in parenthesis in (7.41) tends to zero as  $T \rightarrow \infty$  by (7.37).

Recall from (7.10), (7.26)  $G(T; \beta) \approx G^{(0)}(\tau_2) + \beta^2 G^{(2)}(T, \tau_2)$ . By (7.41),  $\beta^2 G^{(2)}(T, \tau_2) = \beta^2 o(T) \times G^{(0)}(\tau_2)$  for  $T \rightarrow \infty$ . Therefore,

$$G(T; \beta) \approx (1 + \beta^2 o(T)) G^{(0)}(\beta^2 T) = (1 + \beta^2 o(T)) e^{(-\Gamma + i\Lambda)\beta^2 T}, \quad (7.42)$$

which satisfies (7.12) through order  $\beta^2$ .

Finally  $\alpha^{(2)}$ , which satisfies (7.29b), can be bounded using the bound on  $\alpha^{(1)}$  in (7.28), Proposition 7.2 and Theorem 7.1. Together with (7.42) we have verified that our approximate solution

$$G \approx G^{(0)} + \beta G^{(1)} + \beta^2 G^{(2)}, \quad (7.43)$$

$$\alpha_d \approx \alpha^{(0)} + \beta \alpha^{(1)} + \beta^2 \alpha^{(2)} \quad (7.44)$$

satisfies (7.12), (7.13). This completes our derivation of the radiation damping effect on the time-scale  $\beta^{-2}$ .

## 8. PROOF OF THE TIME DECAY ESTIMATE OF PROPOSITION 7.1

We prove the following: There exists  $\rho > 0$  and  $r > 0$  such that for any  $f \in \mathcal{S}(\mathbb{R})$  we have

$$\sup_{t \geq 0} t^\rho \left\| \langle x \rangle^{-r} \frac{e^{-i\mathcal{D}_0 t}}{i(\mathcal{D}_0 - \omega + i0)} \mathcal{P}_c f \right\|_{L^2} < \infty. \quad (8.1)$$

Here,  $\mathcal{P}_c$  denotes the continuous (dispersive) spectral part of  $\mathcal{D}_0$ .

Bounds similar to (8.1) are proved in [40] for scalar 3D Klein-Gordon equations with spatially varying and decaying potentials. Our strategy is to make an algebraic reduction to a problem of this type and to apply appropriate 1D dispersive estimates. In particular, to prove (8.1) (and hence the decay of  $\Upsilon_1(t)$ , see (7.35)), we shall re-express  $e^{-i\mathcal{D}_0 t}$  in terms of a diagonal Klein-Gordon evolution operators to which we can apply known time-decay estimates.

We begin with the an algebraic observation.

**Lemma 8.1.** (1)

$$\mathcal{D}_0^2 = S \mathcal{D} S^*, \quad (8.2)$$

where

$$S \equiv \frac{1}{2} \begin{pmatrix} 1 & 1 \\ i & -i \end{pmatrix}, \quad \mathcal{D} \equiv \begin{pmatrix} Z_+ & 0 \\ 0 & Z_- \end{pmatrix},$$

and

$$Z_\pm \equiv -v_D \partial_X^2 + \vartheta_\pm^2 \kappa^2(X) \pm v_D \vartheta_\pm \kappa'(X).$$

(2) For any continuous function  $\phi$  on the spectrum of  $\mathcal{D}_0^2$ ,

$$\phi(\mathcal{D}_0^2) P_c(\mathcal{D}_0) = S \phi(\mathcal{D}) S^*$$

Note that  $Z_+$  and  $Z_-$  are non-negative self-adjoint operators, by (8.2). It is also useful to note that  $Z_+$  and  $Z_-$  can be expressed as spatially localized perturbations of the constant coefficient operator

$$Z_0 = -\partial_x^2 + \kappa_\infty^2; \quad \text{namely,} \quad (8.3)$$

$$Z_\pm = Z_0 + \vartheta_\sharp^2(\kappa^2(X) - \kappa_\infty^2) \pm v_D \vartheta_\sharp \kappa'(X) \quad (8.4)$$

*Proof of Lemma 8.1.* Using the commutation relation  $\sigma_3 \sigma_1 = -\sigma_1 \sigma_3$ , we obtain

$$\begin{aligned} \mathcal{D}_0^2 &= (iv_D \sigma_3 \partial_X + \vartheta_\sharp \kappa(X) \sigma_1)^2 \\ &= I(-v_D^2 \partial_X^2 + \vartheta_\sharp^2 \kappa^2(X)) + v_D \vartheta_\sharp \sigma_2 \kappa'(X). \end{aligned}$$

Hence,  $\mathcal{D}_0^2$  is diagonalizable using the eigenvectors of  $\sigma_2$ . In particular,  $S \sigma_2 = \sigma_3 S$  which implies (8.2)  $\square$

Define  $\mathcal{P}_+ \equiv \mathcal{P}_c(\mathcal{D}_0 > 0)$  and  $\mathcal{P}_- \equiv \mathcal{P}_c(\mathcal{D}_0 < 0)$  so that  $\mathcal{P}_c = \mathcal{P}_+ + \mathcal{P}_-$ .

**Proposition 8.1.**

$$\mathcal{D}_0 \mathcal{P}_\pm f = \pm S \mathcal{D}^{\frac{1}{2}} S^* \mathcal{P}_\pm$$

and, in particular,

$$\frac{e^{-i\mathcal{D}_0 t}}{i(\mathcal{D}_0 - \omega + i0)} P_\pm f = S \frac{e^{\mp i\mathcal{D}^{\frac{1}{2}} t}}{i(\pm \mathcal{D}^{\frac{1}{2}} - \omega + i0)} S^* P_\pm f. \quad (8.5)$$

*Proof of Proposition 8.1.* Since  $\mathcal{D}$  is similar to the positive semi-definite  $\mathcal{D}_0^2$  (positive definite on its continuous part), we have  $\mathcal{D}_0 \mathcal{P}_\pm f = \pm (S \mathcal{D} S^*)^{\frac{1}{2}} \mathcal{P}_\pm f$ . For simplicity, we restrict our attention to  $f \in \text{Range}(\mathcal{P}_+)$ . The case where  $f \in \text{Range}(\mathcal{P}_-)$  negative case follows analogously.

Recall that for any positive-semidefinite operator  $A$

$$A^{\frac{1}{2}} = cA \int_0^\infty z^{-\frac{1}{2}} (zI + A)^{-1} dz.,$$

where  $c > 0$  is an appropriately chosen constant. Therefore

$$\begin{aligned} (S \mathcal{D} S^*)^{\frac{1}{2}} &= S \mathcal{D} S^* c \int_0^\infty z^{-\frac{1}{2}} (zI + S \mathcal{D} S^*)^{-1} dz \\ &= S \mathcal{D} S^* c \int_0^\infty z^{-\frac{1}{2}} (S(zI + \mathcal{D}) S^*)^{-1} dz \\ &= S \mathcal{D} S^* S \left[ c \int_0^\infty z^{-\frac{1}{2}} (zI + \mathcal{D})^{-1} dz \right] S^* = S \mathcal{D}^{\frac{1}{2}} S^*. \end{aligned}$$

Hence,  $\mathcal{D}_0 \mathcal{P}_\pm f = \pm S \mathcal{D}^{\frac{1}{2}} S^* \mathcal{P}_\pm$ . The equation (8.5) now follows.  $\square$

**8.1. Proof of Proposition 7.1, time-decay estimate (8.1).** Let  $J$  be a non-empty open interval in  $\mathbb{R}$  containing zero and let  $\chi_J(y)$  denote a smooth out characteristic function with support in  $J$ . The support of  $J$  will be fixed below. We write  $\mathbb{R} = J + J^c$  and hence  $1 = \chi_J(y) + \chi_{J^c}(y)$ . Therefore,

$$\begin{aligned} \left\| \langle x \rangle^{-r} S \frac{e^{-i\mathcal{D}^{\frac{1}{2}}t}}{i(\mathcal{D}^{\frac{1}{2}} - \omega + i0)} S^* \mathcal{P}_+ f \right\|_{L^2} &\leq \text{Term I} + \text{Term II}, \quad \text{where} \\ \text{Term I} &\equiv \left\| \langle x \rangle^{-r} S \frac{e^{-i\mathcal{D}^{\frac{1}{2}}t}}{i(\mathcal{D}^{\frac{1}{2}} - \omega + i0)} \chi_J(|\mathcal{D}^{\frac{1}{2}} - \omega|) S^* \mathcal{P}_+ f \right\|_{L^2} \quad (8.6) \\ \text{Term II} &\equiv \left\| \langle x \rangle^{-r} S \frac{e^{-i\mathcal{D}^{\frac{1}{2}}t}}{i(\mathcal{D}^{\frac{1}{2}} - \omega + i0)} \chi_{J^c}(|\mathcal{D}^{\frac{1}{2}} - \omega|) S^* \mathcal{P}_+ f \right\|_{L^2} \quad (8.7) \end{aligned}$$

We next estimate the expressions Term I and Term II. In particular, we show that for any  $N$ , there exists  $r = r(N)$  such that

$$\text{Term I} \leq t^{-N} \|\langle x \rangle^N f\|_{L^2}, \quad (8.8)$$

$$\text{Term II} \leq t^{-\frac{1}{4}} \|f\|_{W^{1,\frac{4}{3}}} \quad (8.9)$$

We first bound Term II and then Term I.

## 8.2. Time-decay estimates for Term II, given by (8.7).

Let  $q^{-1} + (p')^{-1} = 1/2$ . Then,

$$\begin{aligned} \text{Term II} &= \left\| \langle x \rangle^{-r} S \frac{e^{-i\mathcal{D}^{\frac{1}{2}}t}}{i(\mathcal{D}^{\frac{1}{2}} - \omega + i0)} \chi_{J^c}(|\mathcal{D}^{\frac{1}{2}} - \omega|) S^* P_+ f \right\|_{L^2} \\ &\leq \|\langle x \rangle^{-r}\|_{L^q} \left\| S \frac{e^{-i\mathcal{D}^{\frac{1}{2}}t}}{i(\mathcal{D}^{\frac{1}{2}} - \omega + i0)} \chi_{J^c}(|\mathcal{D}^{\frac{1}{2}} - \omega|) S^* P_+ f \right\|_{L^{p'}}. \end{aligned}$$

Next, we prove a time-decay estimate for the latter factor.

For  $j = +, -$ , introduce wave operators  $W_j$  which intertwine each  $Z_j$  on its continuous spectral part [42, 43], i.e.,  $\mathcal{D}_j \mathcal{P}_c(Z_j) = W_j Z_0 W_j^*$ , and define the block diagonal operator  $W = \text{diag}(W_+, W_-)$ . For any Borel measurable function,  $\phi$ , we have

$$\phi(Z_\pm) \mathcal{P}_c(Z_\pm) = W_\pm \phi(Z_0) W_\pm^*, \quad (8.10)$$

and hence for matrix operator-valued Borel functions

$$\phi(\mathcal{D}) \mathcal{P}_c(\mathcal{D}) = W \phi(Z_0 \sigma_0) W^*,$$

where  $\sigma_0$  is the  $2 \times 2$  identity matrix. Therefore,

$$\phi(\mathcal{D}_0^2) P_c(\mathcal{D}_0) = S \phi(\mathcal{D}) \mathcal{P}_c(\mathcal{D}) S^* = S W \phi(\mathcal{D}_0) (S W)^*, \quad (8.11)$$

where  $\mathcal{D}_0 = \sigma_0 Z_0$ . In particular,  $(S W) (S W)^* = \mathcal{P}_c(\mathcal{D}_0)$ .

As shown in [42, 43] the wave operators  $W_j$ , and hence  $W$ , are bounded in  $W^{k,p}(\mathbb{R}^n)$ . This then allows us to reduce decay estimates for  $e^{-i\mathcal{D}^{\frac{1}{2}}t} \mathcal{P}_c(\mathcal{D})$  to

those for  $e^{-iZ_0^{\frac{1}{2}}t}$ . Therefore, we have with  $p^{-1} + (p')^{-1} = 1$ :

$$\begin{aligned} \text{Term II} &\lesssim \left\| SW \frac{e^{-i\mathcal{D}_0^{\frac{1}{2}}t}}{i(\mathcal{D}_0^{\frac{1}{2}} - \omega + i0)} \chi_{J^c}(|\mathcal{D}_0^{\frac{1}{2}} - \omega|) (SW)^* f \right\|_{L^{p'}} \\ &\lesssim \left\| \frac{e^{-i\mathcal{D}_0^{\frac{1}{2}}t}}{i(\mathcal{D}_0^{\frac{1}{2}} - \omega + i0)} \chi_{J^c}(|\mathcal{D}_0^{\frac{1}{2}} - \omega|) (SW)^* f \right\|_{L^{p'}} \\ &\lesssim \left\| e^{-i\mathcal{D}_0^{\frac{1}{2}}t} \right\|_{L^{p'} \leftarrow W^{1,p}} \left\| (\mathcal{D}_0^{\frac{1}{2}} - \omega)^{-1} \chi_{J^c}(|\mathcal{D}_0^{\frac{1}{2}} - \omega|) (SW)^* f \right\|_{W^{1,p}} \\ &\lesssim \left\| e^{-i\mathcal{D}_0^{\frac{1}{2}}t} \right\|_{L^{p'} \leftarrow W^{1,p}} \left\| \mathcal{D}_0^{\frac{1}{2}} (\mathcal{D}_0^{\frac{1}{2}} - \omega)^{-1} \chi_{J^c}(|\mathcal{D}_0^{\frac{1}{2}} - \omega|) (SW)^* f \right\|_{L^p} \\ &\lesssim \left\| e^{-i\mathcal{D}_0^{\frac{1}{2}}t} \right\|_{L^{p'} \leftarrow W^{1,p}} \left\| \mathcal{D}_0^{\frac{1}{2}} (\mathcal{D}_0^{\frac{1}{2}} - \omega)^{-1} \chi_{J^c}(|\mathcal{D}_0^{\frac{1}{2}} - \omega|) \right\|_{L^p \leftarrow L^p} \left\| (SW)^* f \right\|_{L^p}. \end{aligned}$$

The second factor just above is bounded because it can be expressed in terms of a Fourier multiplier on  $L^p$  and the third factor is controlled by  $\|f\|_{L^p}$  by boundness of wave operators. Hence,

$$\text{Term II} \lesssim \left\| e^{-i\mathcal{D}_0^{\frac{1}{2}}t} \right\|_{W^{1,p} \rightarrow L^{p'}} \|f\|_{L^p} \lesssim \left\| e^{-iZ_0^{\frac{1}{2}}t} \right\|_{W^{1,p} \rightarrow L^{p'}} \|f\|_{L^p}$$

Dispersive time-decay estimates for the 1D Klein-Gordon equation yield:

$$\|e^{-iZ_0^{\frac{1}{2}}t} f\|_{L^\infty} \leq t^{-1/2} \|(I - \partial_x^2)^{\frac{1}{4}} f\|_{L^1}, \quad t \gg 1;$$

for general results, see, e.g., [12]. Together with the unitarity of the Klein-Gordon flow  $\|e^{-iZ_0^{\frac{1}{2}}t} f\|_{L^2} = \|f\|_{L^2}$  we have, using interpolation, that

$$\begin{aligned} \|e^{-iZ_0^{\frac{1}{2}}t} f\|_{L^{p'}} &\lesssim \|e^{-iZ_0^{\frac{1}{2}}t} f\|_{L^2}^{\frac{2}{p'}} \cdot \|e^{-iZ_0^{\frac{1}{2}}t} f\|_{L^\infty}^{1 - \frac{2}{p'}} \\ &\lesssim \|f\|_{L^2}^{\frac{2}{p'}} \cdot \left( t^{-\frac{1}{2}} \|(I - \partial_x^2)^{\frac{1}{4}} f\|_{L^1} \right)^{1 - \frac{2}{p'}} \\ &\lesssim t^{-\frac{1}{2} + \frac{1}{p'}} \|f\|_{L^2}^{\frac{2}{p'}} \cdot \|f\|_{W^{\frac{1}{2},1}}^{1 - \frac{2}{p'}} \end{aligned}$$

where  $p^{-1} + (p')^{-1} = 1$ . Finally, let us fix  $p = 4/3$  and  $p' = 4$ . Then, we have that

$$\text{Term II} \leq t^{-\frac{1}{4}} \|f\|_{L^{\frac{4}{3}}} \cdot \|f\|_{L^2}^{\frac{1}{2}} \cdot \|f\|_{W^{\frac{1}{2},1}}^{\frac{1}{2}}.$$

### 8.3. Time decay estimate for Term I given by (8.6).

Recall that

$$\text{Term I} \equiv \left\| \langle x \rangle^{-r} S \frac{e^{-i\mathcal{D}^{\frac{1}{2}}t}}{i(\mathcal{D}^{\frac{1}{2}} - \omega + i0)} \chi_J(|\mathcal{D}^{\frac{1}{2}} - \omega|) S^* P_+ f \right\|_{L^2}$$

Noting that, using integration by parts,

$$\begin{aligned} &\frac{e^{i\mathcal{D}^{\frac{1}{2}}t}}{i(\mathcal{D}^{\frac{1}{2}} - \omega + i0)} \chi_J(|\mathcal{D}^{\frac{1}{2}} - \omega|) S^* P_+ \\ &= - \lim_{\varepsilon \rightarrow 0^+} e^{-i(\omega + i\varepsilon)t} \int_t^\infty e^{-i(\mathcal{D}^{\frac{1}{2}} - \omega + i\varepsilon)\tau} \chi_J(|\mathcal{D}^{\frac{1}{2}} - \omega|) S^* P_+ \, d\tau, \end{aligned} \quad (8.12)$$

it suffices to show sufficient decay of an appropriate operator norm of the integrand of (8.12). Since we have  $\mathcal{D} = \text{diag}(Z_+, Z_-)$ , time-decay bounds of the integrand in (8.12) can be reduced to  $e^{-iZ_\pm t} P_c(Z_\pm)$ . The Mourre approach to scattering estimates, as applied in [40, Section 2], yields

$$\|\langle x \rangle^{-r} S e^{-i\mathcal{D}^{\frac{1}{2}}\tau} \chi_J(|\mathcal{D}^{1/2} - \omega|) S^* P_+ f\|_{L^2} \lesssim \left( \langle t \rangle^{-r} + \langle t \rangle^{-N/2} \right) \|\langle x \rangle^{N/2} f\|_{L^2}, \quad N \in \mathbb{N} \quad (8.13)$$

where  $r$  and  $N$  can be taken large. The desired bound on the expression Term I (see (8.6)) now follows from estimating the integrand of (8.12) using (8.13) and integrating.

With the estimates (8.8) and (8.9) on Term I and Term II now proved, the proof of Proposition 7.1 is now complete.

#### APPENDIX A. DERIVATION OF THE EFFECTIVE DIRAC EQUATION

Introduce  $X = \varepsilon x$  and  $T = \varepsilon t$ , the slow space and time variables, respectively. Formally, we view  $\psi$  as dependent on all four variables, i.e., we seek  $\Psi(t, T, x, X)$  such that  $\psi(t, x)$ , the true solution of the Schrödinger equation (3.12), is well approximated by  $\Psi(t, T, x, X)|_{T=\varepsilon t, X=\varepsilon X}$ . Hence,  $\partial_x \mapsto \partial_x + \varepsilon \partial_X$  and  $\partial_t \mapsto \partial_t + \varepsilon \partial_T$ , and (3.12) is rewritten into

$$i(\partial_t - H_0)\Psi(t, x, T, X) = \varepsilon H_1 \Psi + \varepsilon^2 H_2 \Psi, \quad (\text{A.1a})$$

where  $H_0 = -\partial_x^2 + V(x)$  as usual, and

$$H_1 \equiv -(i\partial_T + 2\partial_x \partial_X + \kappa(X)W(x) + 2i\beta A(T)\partial_x), \quad H_2 \equiv -(\partial_X^2 + 2i\beta A(T)\partial_X). \quad (\text{A.1b})$$

Since we are looking for wavepackets which are spectrally centered at the Dirac point, the boundary conditions (or function space) in which we solve (A.1) is  $k_D = \pi$ -pseudo periodicity in  $x$  and  $L_X^2(\mathbb{R})$  in  $X$ .

We seek  $\Psi$  as an expansion in orders of  $\varepsilon$ ,

$$\psi = \psi^{(0)}(t, T, x, X) + \varepsilon \psi^{(1)}(t, T, x, X) + \varepsilon^2 \psi^{(2)}(t, T, x, X) + \dots \quad (\text{A.2})$$

Substituting (A.2) into (A.1) and collecting terms by orders of  $\varepsilon$ , at the  $\varepsilon^0$  order we obtain the initial value problem

$$(i\partial_t - H_0)\psi^{(0)} = 0, \quad (\text{A.3a})$$

$$\psi^{(0)}(0, 0, x, X) = \alpha_{*,1}(X)\Phi_1(x; k_D) + \alpha_{*,2}(X)\Phi_2(x; k_D), \quad (\text{A.3b})$$

with  $\alpha_* \in L_X^2(\mathbb{R}; \mathbb{C}^2)$  as defined in (3.5).<sup>8</sup> As noted in Section 3.1, the  $L_{k_D}^2$ -nullspace of  $E_D I - H_{\text{bulk}}$  is spanned by the Bloch modes  $\{\Phi_1, \Phi_2\}$ , and so the solution of (A.3) is given by

$$\psi^{(0)} = e^{-iE_D t} \sum_{j=1}^2 \alpha_j(T, X)\Phi_j(x), \quad (\text{A.4})$$

where  $\alpha_1(T, X)$  and  $\alpha_2(T, X)$  are rapidly-decaying functions yet to be determined with  $\alpha_j(0, X) = \alpha_{*,j}(X)$  for  $j = 1, 2$ .

<sup>8</sup>Admittedly, the initial condition  $\psi_*$  is only well-approximated by  $\alpha_*^\top \Phi$ , but since we are only formally expanding the initial value problem and disregard small error term, we can take this approximation in (A.3b).

Proceeding to order  $\varepsilon$ , we obtain

$$(i\partial_t - H_0)\psi^{(1)} = (-i\partial_T - 2\partial_x\partial_X + \kappa(X)W(x) + 2iA(T)\partial_x)\psi^{(0)}. \quad (\text{A.5})$$

Since  $\psi^{(0)}$  oscillates with frequency  $E_D$ , it will be convenient to extract the fast oscillatory behavior of  $\psi^{(1)}$  by defining

$$\psi^{(1)}(t, T, x, X) = e^{-iE_D t}\tilde{\psi}^{(1)}(T, x, X).$$

Substituting the above ansatz and (A.4) into (A.5), we obtain

$$\begin{aligned} (E_D I - H_0)\tilde{\psi}^{(1)}(T, x, X) &= -\sum_{j=1}^2 \partial_T \alpha_j(T, X) \Phi_j + i \sum_{j=1}^2 \partial_X \alpha_j \cdot 2i\partial_x \Phi_j \\ &+ \sum_{j=1}^2 \kappa(X) \alpha_j W(x) \Phi_j + \sum_{j=1}^2 \beta A(T) \alpha_j \cdot 2i\partial_x \Phi_j. \end{aligned} \quad (\text{A.6})$$

The solvability of (A.6) for  $\tilde{\psi}^{(1)} \in L^2_{k_D}$  requires the  $L^2_{k_D}$ -orthogonality of its right-hand side to  $\Phi_1$  and  $\Phi_2$ . In [10, Proposition 2.2], it is shown that

$$\begin{pmatrix} \langle \Phi_1, 2i\partial_x \Phi_1 \rangle & \langle \Phi_2, 2i\partial_x \Phi_1 \rangle \\ \langle \Phi_1, 2i\partial_x \Phi_2 \rangle & \langle \Phi_2, 2i\partial_x \Phi_2 \rangle \end{pmatrix} = v_D \sigma_3, \quad (\text{A.7a})$$

$$\begin{pmatrix} \langle \Phi_1, W \Phi_1 \rangle & \langle \Phi_2, W \Phi_1 \rangle \\ \langle \Phi_1, W \Phi_2 \rangle & \langle \Phi_2, W \Phi_2 \rangle \end{pmatrix} = \vartheta_{\sharp} \sigma_1, \quad (\text{A.7b})$$

where  $v_D, \vartheta_{\sharp} \neq 0$ . Thus, the solvability conditions reduce to

$$i\partial_T \alpha_1 = \langle \Phi_1, 2i\partial_x \Phi_1 \rangle (i\partial_X + \beta A(T)) \alpha_1 + \langle \Phi_1, W \Phi_2 \rangle \kappa(X) \alpha_2,$$

$$i\partial_T \alpha_2 = \langle \Phi_2, 2i\partial_x \Phi_2 \rangle (i\partial_X + \beta A(T)) \alpha_2 + \langle \Phi_2, W \Phi_1 \rangle \kappa(X) \alpha_1,$$

from which we obtain the Dirac equation

$$i\partial_T \alpha(T, X) = (iv_D \sigma_3 \partial_X + \vartheta_{\sharp} \kappa(X) \sigma_1 + v_D \beta A(T) \sigma_3) \alpha.$$

with  $\alpha(0, X) = \alpha_{\star}(X)$ , as first introduced in (5.1).

## APPENDIX B. THE POTENTIALS $U_{\varepsilon}^{(\ell)}$ AND THEIR EFFECTIVE DIRAC HAMILTONIANS

To construct  $U_{\varepsilon}^{(1)}$ , we choose  $V(x) = \cos(4\pi x)$ ,  $W(x) = \cos(2\pi x)$ ,  $\kappa(X) = \tanh(X)$ ,  $A(T) = \cos(\omega T)$ , and  $\varepsilon = \frac{1}{2}$ . The initial value problem (3.12) becomes

$$i\partial_t \psi = [-\partial_x^2 + \cos(4\pi x) + \frac{1}{2} \tanh(\frac{1}{2}x) \cos(2\pi x) + i\beta \cos(\frac{1}{2}\omega t) \partial_x] \psi, \quad (\text{B.1a})$$

$$\psi(0, x) = \psi_{\star}(x), \quad (\text{B.1b})$$

where  $\beta, \omega > 0$ . The potential  $U_{\varepsilon}^{(2)}$  models a chain of isolated and dimerized square wells, a more realistic model for an array of coiled optical waveguides as in Fig. 3. Let  $\Theta(x; a)$  be a square function of radius  $1 \gg a > 0$

$$\Theta(x; a) \equiv \begin{cases} 1, & |x| \leq a, \\ 0, & |x| > a. \end{cases}$$

and define

$$Q_{\pm}(x; a) \equiv \sum_{z \in \mathbb{Z}} \Theta(x + z; a) \pm \Theta(x + z + \frac{1}{2}; a). \quad (\text{B.2})$$

We choose  $V(x) = -5Q_+(x; \frac{1}{20})$ ,  $W(x) = -5Q_-(x; \frac{1}{20})$ ,  $\kappa = \kappa_{\text{pw}}$  where

$$\kappa_{\text{pw}}(y) \equiv \begin{cases} 0, & 0 \leq y < y_0, \\ \frac{1}{2}, & y_0 \leq y < 2y_0, \\ 1, & y \geq 2y_0, \\ -\kappa_{\text{pw}}(-y), & y < 0, \end{cases} \quad y_0 \equiv \tanh^{-1}(\frac{1}{2}) \approx 0.549. \quad (\text{B.3})$$

Hence, the initial value problem (3.12) becomes

$$i\partial_t \psi(x, t) = \left[ -\partial_x^2 - 5Q_+(x; \frac{1}{20}) - \frac{5}{2}\kappa_{\text{pw}}(\frac{1}{2}x)Q_-(x; \frac{1}{20}) + i\beta \cos(\frac{1}{2}\omega t)\partial_x \right] \psi. \quad (\text{B.4})$$

The potential  $U_\varepsilon^{(3)}$  is similar to  $U_\varepsilon^{(2)}$ , and the only change is that we now set  $\kappa(X) = \text{sgn}(X + 1/2)$ , the signum function, where the shift is introduced so as to avoid changes in the middle of one of the potential wells.

$$i\partial_t \psi(x, t) = \left[ -\partial_x^2 - 5Q_+(x; \frac{1}{20}) - \frac{5}{2}\text{sgn}(x + \frac{1}{4})Q_-(x; \frac{1}{20}) + i\beta \cos(\frac{1}{2}\omega t)\partial_x \right] \psi. \quad (\text{B.5})$$

The corresponding Dirac Hamiltonians are denoted by  $D_0^{(\ell)}$ , where for  $\ell = 1$

$$(\text{5.1}) \text{ with } v_D = 2\pi, \quad \vartheta_\sharp = \frac{1}{2}, \quad \kappa(X) = \tanh(X), \quad (\text{B.6})$$

for  $\ell = 2$

$$(\text{5.1}) \text{ with } v_D \approx 6.45, \quad \vartheta_\sharp \approx 1.03, \quad \kappa(X) = \kappa_{\text{pw}}(X), \text{ see (B.3)}. \quad (\text{B.7})$$

and for  $\ell = 3$

$$(\text{5.1}) \text{ with } v_D \approx 6.45, \quad \vartheta_\sharp \approx 1.03, \quad \kappa(X) = \text{sgn}(X), \text{ see (B.3)}. \quad (\text{B.8})$$

## APPENDIX C. NUMERICAL METHODS

To solve the initial value problems (3.12) and (5.1), we use three-points stencil finite-difference discretization of the Hamiltonians, and the Crank-Nicholson method for time integration [19]. As for boundary conditions, we observe that for a computational domain  $[-L, L]$  with  $L \gg 1$  sufficiently large, both periodic and vanishing boundary conditions yield seemingly identical results. The defect modes  $\psi_*$  and  $\alpha_*$  were both computed using direct diagonalization of the corresponding discretized Hamiltonians.

To derive the Dirac equation (5.1) from the Schrödinger equation (3.12), we compute the parameters  $v_D$  and  $\vartheta_\sharp$  in the following way: first, we construct a second-order finite difference matrix approximation of  $H_{0,k}$ , the Hamiltonian with  $k$  quasi-periodic boundary conditions, see (2.2). The Bloch modes  $\Phi_1$  and  $\Phi_2$  are then the lower-most eigenvectors with  $k = k_D = \pi$ . Second, the inner-products in (3.2) and (A.7b) are computed using a trapezoid quadrature rule.

Finally, whenever curve fitting is required, we use the SciPy `curve_fit` nonlinear least squares framework.

## REFERENCES

1. Mark J Ablowitz, Christopher W Curtis, and Yi-Ping Ma, *Adiabatic dynamics of edge waves in photonic graphene*, 2D Materials **2** (2015), no. 2, 024003.
2. MJ Ablowitz and Cole JT, *Tight-binding methods for general longitudinally driven photonic lattices: Edge states and solitons*, Phys. Rev. Lett. **96** (2017), 043868.
3. Shmuel Agmon, Ira Herbst, and Erik Skibsted, *Perturbation of embedded eigenvalues in the generalized  $n$ -body problem*, Communications in mathematical physics **122** (1989), no. 3, 411–438.

4. János K Asbóth, B Tarasinski, and Pierre Delplace, *Chiral symmetry and bulk-boundary correspondence in periodically driven one-dimensional systems*, Physical Review B **90** (2014), no. 12, 125143.
5. Matthieu Bellec, Claire Michel, Haisu Zhang, Stelios Tzortzakis, and Pierre Delplace, *Non-diffracting states in one-dimensional floquet photonic topological insulators*, EPL (Europhysics Letters) **119** (2017), no. 1, 14003.
6. Jérôme Cayssol, Balázs Dóra, Ferenc Simon, and Roderich Moessner, *Floquet topological insulators*, physica status solidi (RRL)-Rapid Research Letters **7** (2013), no. 1-2, 101–108.
7. Ovidiu Costin and Avraham Soffer, *Resonance theory for schrödinger operators*, Communications in Mathematical Physics **224** (2001), no. 1, 133–152.
8. Virginia Dal Lago, M Atala, and LEF Foa Torres, *Floquet topological transitions in a driven one-dimensional topological insulator*, Physical Review A **92** (2015), no. 2, 023624.
9. A. Drouot, *The bulk-edge correspondence for continuous dislocated systems*, Annales de l’Institut Fourier (2021).
10. Alexis Drouot, Charles L Fefferman, and Michael I Weinstein, *Defect modes for dislocated periodic media*, Communications in Mathematical Physics **377** (2020), no. 3, 1637–1680.
11. MSP Eastham, *The Spectral Theory of Periodic Differential Equations*, Scottish Academic Press, 1973.
12. I. Egorova, E. Kopylova, V. Marchenko, and G. Teschl, *Dispersion estimates for one-dimensional Schrödinger and Klein-Gordon equations revisited*, Russian Mathematical Surveys **71** **71** (2016), no. 3.
13. Charles L Fefferman, James P Lee-Thorp, and Michael I Weinstein, *Topologically protected states in one-dimensional continuous systems and dirac points*, Proceedings of the National Academy of Sciences **111** (2014), no. 24, 8759–8763.
14. Charles L Fefferman and Michael I Weinstein, *Wave packets in honeycomb structures and two-dimensional dirac equations*, Communications in Mathematical Physics **326** (2014), no. 1, 251–286.
15. C.L. Fefferman, J. P. Lee-Thorp, and M. I. Weinstein, *Topologically protected states in one-dimensional systems*, Memoirs of the American Mathematical Society **247** (2017), no. 1173, 1–132.
16. Romain Fleury, Alexander B Khanikaev, and Andrea Alu, *Floquet topological insulators for sound*, Nature communications **7** (2016), no. 1, 1–11.
17. Gian Michele Graf and Clément Tauber, *Bulk-edge correspondence for two-dimensional floquet topological insulators*, Annales Henri Poincaré, vol. 19, Springer, 2018, pp. 709–741.
18. Jonathan Guglielmon, Sheng Huang, Kevin P Chen, and Mikael C Rechtsman, *Photonic realization of a transition to a strongly driven floquet topological phase*, Physical Review A **97** (2018), no. 3, 031801.
19. Arieh Iserles, *A first course in the numerical analysis of differential equations*, no. 44, Cambridge university press, 2009.
20. Sergey K Ivanov, Yaroslav V Kartashov, Matthias Heinrich, Alexander Szameit, Lluis Torner, and Vladimir V Konotop, *Topological dipole floquet solitons*, Physical Review A **103** (2021), no. 5, 053507.
21. Sergey K Ivanov, Yaroslav V Kartashov, Lukas J Maczewsky, Alexander Szameit, and Vladimir V Konotop, *Edge solitons in lieb topological floquet insulator*, Optics letters **45** (2020), no. 6, 1459–1462.
22. Gregor Jotzu, Michael Messer, Rémi Desbuquois, Martin Lebrat, Thomas Uehlinger, Daniel Greif, and Tilman Esslinger, *Experimental realization of the topological haldane model with ultracold fermions*, Nature **515** (2014), no. 7526, 237–240.
23. Marius Jürgensen, Sebabrata Mukherjee, and Mikael C Rechtsman, *Quantized nonlinear thousandless pumping*, Nature **596** (2021), no. 7870, 63–67.
24. E Kirr and MI Weinstein, *Metastable states in parametrically excited multimode hamiltonian systems*, Communications in mathematical physics **236** (2003), no. 2, 335–372.
25. P.A. Kuchment, *An overview of periodic elliptic operators*, Bull. Amer. Math. Soc. **53** (2016), no. 3, 343–414.
26. J. P. Lee-Thorp, I. Vukićević, X. Xu, J. Yang, C. L. Fefferman, C. W. Wong, and M. I. Weinstein, *Photonic realization of topologically protected bound states in domain-wall waveguide arrays*, Phys. Rev. A **93** (2016), 033822.

27. Jianfeng Lu, Alexander B Watson, and Michael I Weinstein, *Dirac operators and domain walls*, SIAM Journal on Mathematical Analysis **52** (2020), no. 2, 1115–1145.
28. Peter D Miller, A Soffer, and Michael I Weinstein, *Metastability of breather modes of time-dependent potentials*, Nonlinearity **13** (2000), no. 3, 507.
29. Sebabrata Mukherjee and Mikael C Rechtsman, *Observation of floquet solitons in a topological bandgap*, Science **368** (2020), no. 6493, 856–859.
30. Tomoki Ozawa, Hannah M Price, Alberto Amo, Nathan Goldman, Mohammad Hafezi, Ling Lu, Mikael C Rechtsman, David Schuster, Jonathan Simon, Oded Zilberberg, et al., *Topological photonics*, Reviews of Modern Physics **91** (2019), no. 1, 015006.
31. Y Plotnik, M C Rechtsman, D Song, M Heinrich, J M Zeuner, S Nolte, Y Lumer, N Malkova, J Xu, A Szameit, Z Chen, and M Segev, *Observation of unconventional edge states in ‘photonic graphene’*, Nature materials **13** (2014), 57–62.
32. Mikael C Rechtsman, Julia M Zeuner, Yonatan Plotnik, Yaakov Lumer, Daniel Podolsky, Felix Dreisow, Stefan Nolte, Mordechai Segev, and Alexander Szameit, *Photonic floquet topological insulators*, Nature **496** (2013), no. 7444, 196–200.
33. M. Reed and B. Simon, *Methods of modern mathematical physics: Analysis of operators, volume iv*, Academic Press, 1978.
34. Rahul Roy and Fenner Harper, *Periodic table for floquet topological insulators*, Physical Review B **96** (2017), no. 15, 155118.
35. Mark S Rudner, Netanel H Lindner, Erez Berg, and Michael Levin, *Anomalous edge states and the bulk-edge correspondence for periodically driven two-dimensional systems*, Physical Review X **3** (2013), no. 3, 031005.
36. Christian Sadel and Hermann Schulz-Baldes, *Topological boundary invariants for floquet systems and quantum walks*, Mathematical Physics, Analysis and Geometry **20** (2017), no. 4, 1–16.
37. Amir Sagiv and Michael I Weinstein, *Effective gaps in continuous floquet hamiltonians*, arXiv preprint arXiv:2105.00958 (2021).
38. JJ Sakurai and Jim Napolitano, *Modern quantum mechanics*, Cambridge University Press, 2020.
39. A. Soffer and M.I. Weinstein, *Time dependent resonance theory*, Geometrical and Functional Analysis **8** (1998), 1086–1128.
40. A Soffer and Michael I Weinstein, *Resonances, radiation damping and instability in hamiltonian nonlinear wave equations*, Inventiones mathematicae **136** (1999), no. 1, 9–74.
41. YH Wang, Hadar Steinberg, Pablo Jarillo-Herrero, and Nuh Gedik, *Observation of floquet-bloch states on the surface of a topological insulator*, Science **342** (2013), no. 6157, 453–457.
42. Ricardo Weder, *Inverse scattering on the line for the nonlinear klein-gordon equation with a potential*, Journal of mathematical analysis and applications **252** (2000), no. 1, 102–123.
43. Kenji Yajima, *The wk, p-continuity of wave operators for schrödinger operators*, Journal of the Mathematical Society of Japan **47** (1995), no. 3, 551–581.

DEPARTMENT OF APPLIED PHYSICS AND APPLIED MATHEMATICS, COLUMBIA UNIVERSITY, NEW YORK, NY 10027, USA

*Email address:* sh3982@columbia.edu

DEPARTMENT OF APPLIED PHYSICS AND APPLIED MATHEMATICS, COLUMBIA UNIVERSITY, NEW YORK, NY 10027, USA

*Email address:* asagiv88@gmail.com

DEPARTMENT OF APPLIED PHYSICS AND APPLIED MATHEMATICS AND DEPARTMENT OF MATHEMATICS, COLUMBIA UNIVERSITY, NEW YORK, NY 10027, USA

*Email address:* miw2103@columbia.edu